The Ocular Albinism type 1 (OA1) G-Protein Coupled Receptor functions with MART-1 at early stages of melanogenesis to control melanosome identity and composition

Journal:	*Human Molecular Genetics*
Manuscript ID:	draft
Manuscript Type:	2 General Article - UK Office
Date Submitted by the Author:	
Complete List of Authors:	Giordano, Francesca; Institut Curie, CNRS UMR144 Bonetti, Ciro; Telethon Institute of Genetics and Medicine, TIGEM Surace, Enrico; Telethon Institute of Genetics and Medicine, TIGEM Marigo, Valeria; University of Modena, Department of Biomedical Sciences Raposo, Graça; Institut Curie, CNRS UMR144
Key Words:	Ocular Albinism, GPCR OA1, melanosome biogenesis, MART-1

The Ocular Albinism type 1 (OA1) G-Protein Coupled Receptor functions with MART-1 at early stages of melanogenesis to control melanosome identity and composition

Francesca Giordano[1,2,], Ciro Bonetti[3], Enrico M. Surace[3], Valeria Marigo[4] and Graça Raposo[,1,2].

[1]Institut Curie, Centre de Recherche, Paris, F-75248 France;

[2] Structure and Membrane Compartments CNRS, UMR144, Paris, F-75248 France

[3] Telethon Institute of Genetics and Medicine, TIGEM, Naples, Italy

[4] Department of Biomedical Sciences, University of Modena and Reggio Emilia, Modena, Italy

[§] corresponding authors:

Graça Raposo

tel: +33 1 56 24 64 41

Fax: +33 1 56 24 64 21

graposo@curie.fr

Valeria Marigo:

tel:+390592055392

fax:+390592055410

valeria.marigo@unimore.it

ABSTRACT

OA1 (GPCR143), the protein product of the ocular albinism type 1 gene, encodes a pigment-cell specific G Protein-Coupled Receptor (GPCR) that localizes intracellularly to melanosomes. OA1 mutations result in ocular albinism due to alterations in melanosome formation, suggesting that OA1 is a key player in the biogenesis of melanosomes. To address the function of OA1 in melanosome biogenesis we have used siRNA inactivation and combined morphological and biochemical methods to investigate melanosome ultrastructure, melanosomal protein localization and expression in human pigmented melanocytic cells. OA1 loss of function leads to decreased pigmentation and causes formation of enlarged aberrant premelanosomes harboring disorganized fibrillar structures and displaying proteins of mature melanosomes and lysosomes at their membrane. Moreover we show that OA1 interacts biochemically with the premelanosomal protein MART-1. Inactivation of MART-1 by siRNA leads to a decreased stability of OA1 and is accompanied by similar defects in premelanosome biogenesis and composition. These data show for the first time that melanosome composition and identity are regulated at early stages by OA1 and that MART-1 likely acts as an escort protein for this GPCR.

Introduction

Albinism comprises a heterogeneous group of inherited genetic disorders characterized by a variable loss of pigmentation in the eye, hair or skin. Ocular albinism type 1 (OA1) is an X-linked disorder that, differently from other forms of albinisms, is not caused by impairment of melanin production but by reduced number of melanosomes (1), the organelles in which melanin is synthesized and stored in Retinal Pigment Epithelium (RPE) and skin melanocytes. Mutations in OA1 gene also induce formation of aberrant "giant" melanosomes, called macromelanosomes (2). Thus, this form of albinism appears to be caused by a defect in melanosome organellogenesis. The protein product of the OA1 gene is a pigment cell specific G protein-coupled receptor (GPCR) (3-6). Differently to canonical GPCR, OA1 preferentially localizes to intracellular compartments such as melanosomes and lysosomes where it can signal from the organelle lumen to the cytosol (4, 7). Although the genetic defect was reported more than 10 years ago (8), how OA1 functions to control melanosome biogenesis has remained enigmatic, frustrating efforts toward development of new therapeutic strategies for ocular albinism.

Melanosomes are lysosome-related organelles that are distinct from conventional lysosomes within pigment cells (9, 10). Melanosomes develop through sequential maturation stages that can be defined based on morphology and that are enriched in a specific set of protein components (9, 11). Stage I and II melanosomes are characterized by the presence of intralumenal fibrillar sheets (12-14), in which the major component is the fibrillogenic protein Pmel17 (13, 15-17), but lack melanogenic enzymes such as Tyrosinase and Tyrosinase-related proteins. Deposition of black melanin along the fibers is initiated in stage III melanosomes as a consequence of the delivery of melanogenic enzymes to preformed stage II melanosomes. Once formed, the mature stage IV melanosomes are transported to the cell periphery for transfer to neighboring keratinocytes or stored within ocular melanocytes in the retinal pigment epithelium (18, 19).

Stage I premelanosomes correspond to early endosomal vacuoles that serve as intermediates for cargo bound both for lysosomes and melanosomes at different stages. As a first step towards melanosome formation, the transmembrane protein Pmel17 is sorted to intraluminal vesicles (ILVs) of endosomes thereafter called multivesicular bodies (MVBs) (9, 15, 16). Concomitant with the sequestration in ILVs,

Pmel17 is cleaved by a prohormone convertase liberating a fibrillogenic fragment (Mα) in its lumenal domain which leads to the generation of the non-membranous amyloid like fibrillar structures (14, 16, 20). Whereas sorting of Pmel17 appears to be independent of ubiquitylation and of the (Endosomal Sorting Complex Required for Transport) ESCRT-0/ESCRT-I machinery (21), sorting of another melanosomal protein, MART-1 that is similarly sequestered in ILVs of MVBs, appears to require ubiquitylation (22, 23) and ESCRT proteins (21, 24). MART-1 has been reported to interact with Pmel17 (25), but the function of MART-1 in melanogenesis is not well understood.

In this study, we investigated the role of OA1 in melanosome biogenesis addressing its intracellular localization and how loss of function may alter trafficking steps required for melanosome maturation. In addition we investigated how it may exert its role together with other melanosomal proteins. Using a combination of light and electron microscopy and biochemical methods we show that OA1 controls the generation of premelanosomes and that it cooperates with MART-1 for this function. Altogether our data suggest that OA1 functions together with MART-1 to maintain melanosome composition and identity within the endocytic system.

Results

OA1 localizes to immature and mature melanosomes

Previous studies have addressed the subcellular localization of endogenous OA1 or GFP-tagged recombinant OA1 in melanocytic cells (4, 7, 26), but its localization within the distinct melanosomal stages and/or endosomes and lysosomes was not completely resolved. To qualitatively and quantitatively evaluate the subcellular distribution of the endogeneous OA1 protein in the melanocytic cell line MNT-1 we have used immunogold labeling on ultrathin cryosections (IEM). MNT-1 cells resemble untransformed skin melanocytes by expression of mRNAs encoding melanogenic proteins (27) and by ultrastructure, presenting melanosomes at all four stages (9). We have also investigated the localization of recombinant OA1 protein (OA1-Flag or OA1-EGFP) in transfected MNT1 cells (see below, fig S1) and in mouse melan-a immortalized melanocytes (data not shown). Consistent with previous studies, OA1 was detected at the limiting membrane of a small cohort of pigmented melanosomes labeled for the melanosomal enzyme Tyrp1 (stage III-IV) (fig 1A, arrows). Within these mature pigmented melanosomes, OA1 was often associated

with small intraluminal vesicles (arrowhead fig 1A) and was also present at the membrane of cytoplasmic vesicles often located in close proximity to melanosomes (fig 1B, arrowhead). OA1 was detected at the limiting membrane of lysosomes (fig 1E, arrows) and in intraluminal vesicles of late endosomes/Multivesicular Bodies (MVBs) (fig 1E, arrowheads). In agreement with its association with ILVs of MVBs, like other ILV associated membrane proteins such as CD63, OA1 was detected in extracellular exosomes secreted from MNT-1 after 48h of culture (not shown). Although OA1 appeared broadly distributed, our observations revealed that the bulk of OA1 was localized to organelles highly labeled for Pmel17 (fig 1C, 1D, arrows; see quantification in fig 1F) that correspond to stage I and stage II premelanosomes (9). This is consistent with but extends quantitatively the observations reported previously (3) and (7). Similarly to endogenous OA1, the recombinant transfected proteins (OA1-Flag or OA1-EGFP) localize to the distinct melanosomal stages and to lysosomes. However, as compared to the endogenous protein we observed a shift in the localization of OA1 towards more mature melanosomes (fig S1A, S1B, arrows). We also observed that cells expressing higher levels of OA1 were characterized by the presence of large electron-lucent OA1 positive membrane vesicles (350 nm). These vesicular structures were also labeled for Tyrp1, and often localized in close proximity to melanosomes in both human (fig S1A, asterisks) and mouse cells (data not shown). These vesicles were possibly induced by the overexpression of OA1 since they were not observed in Flag/EGFP empty vectors transfected cells (data not shown). The observed phenotype indicates that the trafficking of recombinant OA1 may not fully reflect that of the endogenous protein. However, on the other hand it also suggests a dominant negative effect of OA1 expression that maybe result in the accumulation of transport intermediates whose trafficking may be controlled by OA1.

Altogether these data show that OA1 is widely distributed throughout the endo-melanosomal system but that most of endogenous protein is localized in unpigmented Stage II melanosomes. This finding is in agreement with the suggested function for OA1 at early stages of melanogenesis as we previously proposed (1).

OA1 loss of function affects melanosomal protein trafficking and melanosome size at early stages of biogenesis

To get further insights on the function of OA1, we inactivated OA1 by RNAi in pigmented MNT1 cells and analyzed melanosome morphology and composition right after the loss of OA1 activity. This approach overcomes the limits and/or compensations of immortalized melanocytes from OA1 patients or mice that contain primarily mature organelles and preclude the study of the different sequential events leading to the formation of macromelanosomes.

We designed and tested three oligonucleotides targeting three different regions of the human OA1 mRNA. As a control we have used a non-targeting siRNA. One of the three siRNAs (siRNA #3) was very efficient in reducing the levels of OA1 transcripts (15% siRNA #1, 78% siRNA #2, 95% siRNA #3)(fig 2A) and was used for experiments presented here. Downregulation of endogenous OA1 protein was confirmed by WB and IF (fig 2B-D). We found that mature melanosomes and melanin content in siOA1 MNT1 cells were reduced as much as 50% compared to the cells treated with the control siRNA (fig 2E-G). Analysis at the ultrastructural level, by conventional EM, also showed a reduction of the total number of melanosomes in MNT1 cells depleted of OA1 (fig 2H-K), consistent with the phenotype characterized in ocular albinism mouse model and patients. Although we did not observe the "classical" pigmented macromelanosomes, we found that OA1 depleted MNT1 cells harbor abnormally enlarged organelles with a heterogeneous content that are mixed with normal melanosomes and could possibly correspond to the precursors of the macromelanosomes (fig 2I; fig S2A). These aberrant mixed compartments contains Pmel17 positive fibrils characteristic of immature melanosomes and an electron dense core of melanin (fig 2I, asterisk; fig S2B-C). Similar phenotypes were observed with a second siRNA sequence (siRNA #2) excluding that the phenotype derives from mistargeting. Of note, similar enlarged "mixed" organelles were also observed in OA1 in vitro cultured melanocytes from knockout mouse (melan-Oa1$^{-/-}$) (fig S2D-E). Cells depleted of OA1 also harbored enlarged immature unpigmented melanosomes that had lost the typical striated appearance and whose internal fibrils were clearly disorganized (fig 2I, arrowhead; fig S2A; fig 3B, 3D, 3F). In order to investigate if these morphological alterations were accompanied by a defect in the localization of melanosomal proteins, we analyzed the distribution of melanosomal proteins in OA1 depleted MNT1 cells by IEM. The fibrillar structures apposed to or contained within the abnormal melanosomal structures were highly labeled with an antibody directed

against Pmel17, the major component of the fibrils (fig 3B, arrowhead; fig S2C, arrows). Of note, Tyrp1 that is nearly absent from Pmel17 enriched Stage II premelanosomes in control cells, is detected at high levels at the membrane of the enlarged organelles (fig 3A-B, arrows, see also fig 3F) suggesting an alteration of its trafficking upon OA1 depletion. Another protein that appeared to be mislocalized to the enlarged melanosomal organelles is LAMP-1. LAMP-1 is a lysosomal protein that is present only in small amounts at the membrane of Tyrp1 positive melanosomes ((9) and fig 3C, 3E, arrows). In OA1 depleted cells LAMP1 was abundant in both aberrant enlarged pigmented organelles and normal size melanosomes (fig 3D, 3F, 3G, arrows). Quantification of these observations is shown in Table 1. LAMP1 also accumulated in Tyrp1 positive vacuolar structures (fig 3H, inset) that were reminiscent of the vesicles observed upon OA1-Flag overexpression (fig S1) suggesting that depletion of OA1 or a dominant negative effect may lead to similar phenotypes. It also suggests that OA1 may function at a fusion/fission step regulating Tyrp1 and LAMP1 content of melanosomes. Although the melanin content was generally reduced in siOA1 MNT1 cells, western blot experiments performed in these cells revealed a slight increase of the amount of Tyrp1 in the OA1 depleted cells and no significant differences in the amount of LAMP1 (fig 3I), consistent with a defect in their trafficking and not expression/degradation. To get further insight on the trafficking defects and nature of the organelles affected upon OA1 loss of function, we performed IEM on cells that were allowed to internalize Transferrin (early-recycling endosomes), BSA-gold (endo-lysosomal compartments) or that were incubated with the weak base DAMP, to evaluate the acidity of the organelles (9). Transferrin (data not shown) and the endocytic tracer BSA-gold (BSAG) were not detected in the enlarged organelles (fig S3A-B) and vacuoles (data not shown) indicating that the defects in trafficking and organelle biogenesis caused by OA1 loss of function were not due to aberrant mistargeting within the endosomal system. The enlarged melanosomal organelles appeared to acidic as are premelanosomes in wild type cells as assayed with DAMP (9) (fig S3C-D). However, and despite that DAMP accumulation is not a quantitative assay for pH, these organelles show an increased labeling for the radical DNP (fig S3D), suggesting that they may be slightly more acidic.

OA1 and MART-1 loss of function similarly affect Pmel17 final processing and early melanosome biogenesis.

We next aimed at further investigating how premelanosome biogenesis could be affected by the loss of OA1 function. The major biogenetic component of the stage II fibrils is the pigment cell-specific protein Pmel17. In stage II melanosomes the Pmel17 forms are detectable with HMB45 antibody, which recognizes the Mα fragment and its proteolytic products (28-30) and with Pep13h antibody, recognizing the processed full length (P1, 100kD) and the cleaved forms (Mβ, 26kD and CTF, 10kD) (31).

Enlarged organelles displayed disorganized fibrils and this prompted us to evaluate Pmel17 expression and processing. We did not detect significant changes of Pmel17 transcript levels upon OA1 loss of function (fig S4A). Next we analyzed the different maturation forms of Pmel17 by using HMB45 and Pep13h antibodies. Although Pep13h did not reveal significant differences in the levels of P1 and Mβ (fig 4Ac), an accumulation of Mα fragment (80kD) and a reduction of one of its products (MαC, 35kD) was observed with the HMB45 antibody in both the TX-soluble (fig 4Aa) and TX-insoluble pool (fig 4Ab) of siOA1 cell lysates (fig 4A). The TX-insoluble pool is enriched in amyloid fibers that are insoluble in non-denaturing detergent TX100 (16). Since MαC is considered to be the major form of the HMB45-reactive species within the fibers (29, 30) its reduction is likely to reflect the disorganization of amyloid-like fibers observed in stage II melanosomes in siOA1 MNT1 cells (fig 2I, arrowhead; fig 3D, 3F). These results indicate that although Pmel17 appears to be cleaved in its luminal domain, its final processing to form the MαC fragment is impaired consistent with the altered morphology of the intraluminal contents of the premelanosomal compartment.

Such effects observed upon OA1 depletion were reminiscent of those described in cells that do not express MART-1 (25). MART-1 is an integral membrane melanosomal protein that has been shown to form complexes with Pmel17 and has been suggested to control Pmel17 processing and stability (25). We therefore used siRNA to deplete MART-1 from MNT-1 cells. MART-1 was effectively downregulated (reduction of 90% of detectable MART-1 transcript and protein) (fig 6I and fig 4B). We confirmed that Pmel17 maturation was affected in MART-1 depleted cells and in particular, similarly to OA1 knockdown, we detected accumulation of the Mα fibrillogenic fragment accompanied by a reduction of its subproduct MαC (fig 4B). To better define the compartments affected by MART-1 depletion, we performed

immunogold EM analysis on ultrathin cryosections of siMART-1 MNT1 cells. No normal stage I premelanosomes were found, but we noted the presence of many aberrant enlarged compartments that often appeared as a mixture of striations and electron dense pigment, similar to those observed in siOA1 cells (fig 4D). Interestingly, these compartments contained abnormally large intraluminal vesicles and their Pmel17-positive fibers were disorganized and/or apposed to one or both sides, indicating altered early melanogenesis. We also found that Tyrp1 (fig 4E, 4F, arrows), and LAMP1 (data not shown) accumulated in early Pmel17 positive premelanosomal compartments with concomitant reduction at the melanosomal membrane as compared with the control cells.

Overall these observations show that loss of function of either OA1 or MART-1 leads to an impairment of melanosome biogenesis at its earliest steps and to mis-trafficking of distinct melanosomal proteins likely en route to their final destination, in this case lysosomes or melanosomes. Moreover these results show that MART-1, similarly to OA1, regulates melanosome maturation and in particular the maintenance of melanosomal identity and composition.

MART-1 interacts with OA1 and is required for OA1 stability in MNT1 cells

Based on the data presented so far we hypothesize that either OA1 and MART-1 fulfill a similar redundant function in early melanogenesis or that one of the two proteins affects the function of the other. We thereby evaluated possible interactions between these proteins and investigated the consequences of MART-1 loss of function on OA1 expression and localization.

For this purpose, we immunoprecipitated endogenous OA1 from MNT1 extracts and tested for the presence of MART-1 by immunoblotting. Consistent with our hypothesis, the 18kDa form of MART-1, corresponding to the not-ubiquitylated form (23), was detected in the anti-OA1 immunocomplexes (fig 5A). We confirmed the specificity of this interaction by co-immunoprecipitation of OA1 with Galpha-i3 (data not shown), as already published (4), but not with the melanogenic enzyme Tyrp1 (fig 5A). Although we detected a biochemical interaction between OA1 and MART-1, co-localization, as analyzed by immunofluorescence followed by 3D deconvolution or IEM, was limited to only a small subset of cellular compartments (fig 5B-L). OA1 was distributed in vesicular structures that mainly correspond to immature and mature melanosomes (see also Fig.1), but MART-1 was essentially localized in the perinuclear area in a region that mainly corresponds to the Golgi/TGN and post-Golgi

endosomal compartments (fig 5B-I and 5J). These data were confirmed by IEM, in which OA1 and MART-1 were detected together only within the Golgi, vesicles close to the Golgi apparatus and endosomal compartments (fig 5J, 5K,5L, arrows).

Interestingly, when we analyzed cell lysates from cells in which MART-1 was depleted with siRNA, we found that MART-1 depletion greatly affected OA1 protein expression and distribution, reducing the levels of OA1 protein (fig 6E-H, 6J) but not its transcript (fig 6I). By contrast, MART-1 RNA and protein levels were not affected in the absence of OA1 (fig S4A-B). These observations suggested that MART-1 loss of function induces an increased degradation of OA1. To further test this hypothesis and to investigate the mechanisms involved in its decreased expression/stability, MART-1 depleted cells were treated for 5 hrs with drugs known to inhibit lysosomal (chloroquine) or proteasomal degradation (MG132 or epoxomycin) respectively. Chloroquine is an inhibitor of intra-lysosome catabolism that raises intralysosomal pH disrupting the activity of lysosomal acid hydrolases (32) (33). As analyzed by western blot, in control cells treated with Chloroquine, the levels of OA1 increased after 5hrs of treatment, showing that OA1 generally undergoes a lysosomal degradation. A similar increase of OA1 protein levels was observed in Chloroquine-treated MART-1-depleted cells (fig 6Ka), showing a partial rescue of OA1 protein levels after only 5 hrs of treatment. In order to address whether the proteasome was involved in OA1 degradation, MART-1 depleted cells were then treated with two proteasome inhibitors MG132 or Epoxomycin. MG132 is a widely used potent synthetic inhibitor of a number of proteasome-associated proteases (34) (35). Epoxomycin is a natural proteasome inhibitor highly specific for the 20S proteasome (36). OA1 protein levels did not significantly change in treated versus untreated control cells. On the other hand, in siMART-1 MNT1 cells we observed significantly higher levels of OA1 protein after 5 hrs of incubation with proteasome inhibitors as compared to the siMART1 untreated cells (fig 6Kb-c). These results suggest that, in absence of MART-1, OA1 is likely to follow also a distinct degradation pathway and in particular proteasomal degradation. The stronger effect of MG132 as compared to epoxomycin could be due to the fact that this compound is not specific for proteasome and is also a potent inhibitor of various cysteine proteases and cathepsins (37, 38). Overall, these data show that OA1 stability/expression requires MART-1.

Discussion

Melanosomes represent a class of lysosome-related organelles that coexist with late endosomes and lysosomes within melanocytes and retinal pigment epithelium. The pathways by which melanosomal proteins are diverted from the classical endocytic organelles toward melanosomes and/or differentially targeted to different melanosomal stages are incompletely defined, but are disrupted in several genetic diseases (39). These diseases, leading to defects in melanosome biogenesis and transfer, are due to mutations in genes encoding proteins involved in intracellular trafficking but also mutations in melanosome specific proteins whose functions remain so far unclear (10, 39). We show here that the OA1 functions early in melanosome biogenesis controlling not only melanosome size but also melanosome composition, and thereby appropriate maturation. In addition we show that OA1 stability and function is ensured by its interaction with the premelanosomal protein MART-1 assigning a significant role to this protein in melanosome biogenesis.

OA1 functions in early melanogenesis and melanosome composition

Our studies evidence that the bulk of intracellular OA1 localizes to Pmel17-positive unpigmented premelanosomes. The presence of endogenous OA1 in the precursors of premelanosomes that also display other melanosomal proteins such as Pmel17 and MART-1 (9, 22, 40), suggest a function for this GPCR early in melanogenesis as previously predicted based in our genetic studies (1).

The albinism phenotype caused by OA1 loss of function is characterized not only by the presence of macromelanosomes but also by a reduction in melanin content and the number of melanosomes at early stages of their maturation (1, 41). After 5 days of OA1 inactivation we were able to reproduce the defect in melanosome number but not the "classical" macromelanosome phenotype probably because a longer time is required to complete melanosome maturation. However even after short inactivation (3 to 5 days) we observed abnormal enlarged pigmented structures with a heterogeneous content. These structures display a size similar to macromelanosomes with an average diameter of 0,9-1 μm (1). In addition, several of the enlarged compartments observed in OA1 knocked-down cells, although not fully electron dense like macromelanosomes in melanocytes from OA1 mutant mice, display a mixed content with an "amorphous" melanin core and fibrillar sheets ((2) and fig S2B-E.). For all these reasons we believe that the enlarged

structures observed in si-OA1 cells correspond to the precursors of macromelanosomes. These aberrant compartments could result from fusion of anomalous premelanosomes with mature melanosomes. Otherwise and not mutually exclusive, these compartments could also arise from an improper formation/composition of immature Stage II melanosomes resulting from abnormal fusion of transport intermediates – or from lack of retrograde transport from maturing melanosomes – to remove cargoes like LAMP1. This is supported by our observations that OA1 depleted cells accumulate Tyrp1 containing vesicular structures and that immature melanosomes (stage I-II) displayed consistent amounts of Tyrp1 at their limiting and internal membranes. This melanogenic enzyme is in general absent from Stage I/Stage II unpigmented melanosomes and enriched in pigmented Stage III and Stage IV (9). These observations indicate mistargeting of melanogenic enzymes to immature melanosomes and this event may lead to abnormal pigment synthesis within premelanosomal compartments. These observations can also explain the reduced number of early stage melanosomes observed in OA1 mutant RPE (1). Abnormal protein targeting is not limited to melanogenic enzymes but also to proteins of other cellular organelles such as the lysosomal membrane protein LAMP1. LAMP1 is normally present in lysosomes, it is also detectable at lower amounts in mature melanosomes but absent from immature unpigmented melanosomes (9). The presence of Tyrp1 and LAMP1 in vesicular structures and within Pmel17 positive early melanosomes favors the hypothesis of an "aberrant" fusion of LAMP1 and Tyrp1 loaded vesicles with StageI/Stage II premelanosomes. The nature of the Tyrp1/LAMP1 containing transport intermediates is not totally clear but based on our recent studies they most likely correspond to post Golgi endosomal compartments (24). These studies indicate that endosomes are required intermediates for Tyrp1 transport from the Golgi to the limiting membrane of melanosomes. These endosomal domains are distinct from EEA1 positive early sorting endosomes and appear to be located just downstream of early recycling endosomes as in the absence of functional Tsg101 there is a reduced flux of Tyrp1 via the plasma membrane and accumulation of Tyrp1 in endosomal vacuoles that are also positive for LAMP1 (24) and CD63 (data not shown). The vacuolar structures observed upon OA1 inactivation show similar characteristics, containing both Tyrp1 and LAMP1 but not internalized Transferrin (data not shown) or the endocytic tracer BSAG, consistent with the notion that these are post-Golgi/endosomal intermediates that are placed downstream of the sorting decision point to segregate endosomal

from melanosomal cargo. Similar vesicular structures bearing OA1 at their membrane were observed in OA1 overexpressing cells supporting our hypothesis that OA1 is involved in regulating trafficking of such intermediates. One plausible hypothesis is that OA1 controls their transport/fusion to/with melanosomes. Since we detected the bulk of endogeneous OA1 in immature melanosomes, OA1 possibly functions in these compartments to negatively control a "too early" fusion of transport intermediates before complete maturation of Stage II premelanosomes. In the absence of functional OA1 these transport intermediates aberrantly fuse with immature melanosomal compartments leading to mistargeting of these proteins to their membranes before completion of maturation. Thereby it seems plausible that in melanocytes issued from OA1 mutant mice, pigmented melanosomes rather correspond to immature aberrant organelles, with an inappropriate composition leading to synthesis of melanin pigments in the wrong organelle. This explains the morphological features of melanosomes and macromelanosomes in OA1 mutant cells and maybe underlies the transport defects of melanosomes recently reported in these cells (42).

OA1 and MART-1 similarly influence Pmel17 processing and melanosome maturation

The enlarged premelanosomal compartments harboring Tyrp1 and LAMP1 at their limiting membrane display Pmel17 positive fibrils in their lumen although the fibrils do not appear to be fully organized as in classical Stage II premelanosomes. The premelanosomal protein Pmel17 is properly processed as judged by western blotting and is able to generate fibrils indicating that its cleavage by prohormone convertases is not affected in the absence of functional OA1. However we observed an increased amount of the Mα fragment over MαC indicating that one very last step of its processing required for fibril formation is impaired resulting in abnormally assembled fibrils. The cause of the observed alterations in fibril formation/organization remains unclear. The intralumenal acidification of the aberrant organelles, as assayed with the weak base DAMP, does not appear to be significantly altered as compared to control unpigmented premelanosomes. Although, we cannot exclude that the slightly higher labeling observed in the inactivated cells could be due to a defective deacidification required to progress the fibrils and consequently mature melanosomes. Otherwise, the inefficient processing could also be the consequence of an altered trafficking of the enzymes required for

these last steps of Pmel17 processing. Confirming this hypothesis is difficult at the moment because, although some of the enzymes involved in early steps of Pmel17 processing have been at least partially identified (16, 31), those allowing these final steps of cleavage are still unknown.

Interestingly, a similar alteration of Pmel17 processing was observed in cells in which the premelanosomal protein MART-1 was inactivated. MART-1 has been suggested to control Pmel17 expression, stability, trafficking and processing (25). We show here that in cells in which MART-1 expression was reduced by 90%, Pmel17 processing is affected but not its expression and trafficking. MNT1 cells show only a partial phenotype of that observed in primary human melanocytes and SK-MEL-28 cells (25), however we confirmed MART1 functional relevance in the generation of Pmel17 Mα fragment. In this study we also unraveled a morphological phenotype in MART-1 knocked-down cells: enlarged aberrant premelanosomes with disorganized fibrils and mistargeting of Tyrp1 and LAMP1 to Pmel17 positive organelles. These vesicles are similar to those observed in OA1 depleted cells. Moreover and despite the higher enrichment in premelanosomes, OA1 such as the premelanosomal protein MART-1 is broadly distributed throughout the biosynthetic pathway, mature melanosomes and lysosomes. Interestingly, the ubiquitylation deficient mutant MART-1 is mistargeted to mature melanosomes (23) in a manner similar to the overexpressed OA1 in human and mouse melanocytes (our study). We therefore hypothesized that OA1 and MART-1 could function at a similar step and/or reciprocally regulate each other.

OA1 expression and function requires MART-1 as an escort protein.

Our observations are consistent with the hypothesis that MART-1 is an essential regulator of OA1 expression and function. These two proteins interact biochemically, as shown by co-immunoprecipitation, and this interaction appears to be independent of the reported MART-1/Pmel17 interaction (25) since we did not observed co-immunoprecipitation of OA1 with Pmel17 (data not shown). MART-1 probably functions in the biosynthetic transport/stabilization of OA1 and this indicates that the phenotypes observed in MART1 depleted cells could rather be the consequence of a decreased expression/function of OA1. In the absence of OA1 MART-1 expression was not affected at the RNA and protein levels. In absence of functional MART-1, OA1 expression was not affected at the RNA level but significantly decreased at the protein level as assayed by western blot and

immunofluorescence. We have also shown that in absence of MART-1 OA1 appears to be degraded by a lysosomal pathway involving the ubiquitin/proteasome system. Consistent with this hypothesis, OA1 expression is restored in cells depleted for both MART-1 and Tsg101, a component of the ESCRT machinery involved in degradation of ubiquitinated cargo proteins (data not shown). These observations show for the first time that OA1 can be degraded by Lysosomal/proteasomal degradation similarly to other GPCRs (43, 44). In addition we showed that MART-1 can interact with OA1 early during its biosynthetic pathway acting as an escort protein that helps its stabilization to prevent degradation. Innamorati et al. showed that arrestin induces an accelerated degradation of OA1 in transfected cells (5) and it is commonly accepted that arrestins can directly induce GPCR degradation by a process distinct from internalization i.e. by promoting receptor ubiquitination through recruitment of E3 ligases and subsequent lysosomal and/or proteasomal-mediated destruction (45, 46). Future studies are needed to unravel the relationship of OA1 interaction with MART-1, arrestin and the ESCRT machinery in the regulation of its degradation.

In conclusion, we show that the GPCR OA1 functions in early melanogenesis controlling melanosome size and composition that impacts on their identity and consequent maturation. In addition we evidence that OA1 expression is ensured by its interaction with MART-1 revealing a role for this protein in melanosome biogenesis. Altogether our data sheds light on how OA1 regulates key steps of melanosome formation also unraveling pathways by which melanosomal proteins are diverted from the classical endocytic organelles and/or differentially targeted to different melanosomal stages. These studies have important implications for understanding the pathophysiology of OA1, the involvement of GPCRs in intracellular trafficking and how highly specialized cells exploit intracellular trafficking pathways to generate unique organelles.

Materials and methods

Cell culture, transfection and siRNA depletion

The immortalized Oa1 null (melan-Oa1$^{-/-}$). and wild type melanocytic cell lines were derived from wild type or Oa1^{-}/$^{-}$ mouse skin (42) and maintained in RPMI-1640 supplemented with 10%FCS and 200nM phorbol 12-myristate 13-acetate at 37°C with 10% CO_2. MNT-1 human melanoma cells were maintained as previously described (9). MNT-1, melan-O and melan-a were transfected with plasmid constructs using Lipofectamine 2000 (Invitrogen) following manufacturer's recommendations. Cells were collected and analyzed after 48 h. Transfection in MNT-1 with siRNA duplex oligonucleotides proceeded as reported (21) and according to the manufacturer's instructions. Cells were subjected to two rounds of transfection (day 0 and day 2), were passaged as required, and processed at day 3 or day 5 for real time qPCR, immunofluorescence microscopy, electron microscopy, western blotting and melanin assay.

The sense strands for the indicated double stranded siRNAs (21-mers) were synthesized with the following sequences or derived from the following references. siRNA OA1 #1: 5'- GGA TAT GAA CCA CAC GGA A -3' (Hs_GPR143_6_HP siRNA from QIAGEN); siRNA OA1 #2: 5'- GGC TGT AAA GTA AGT GTA A -3' (Hs_GPR143_3_HP siRNA from QIAGEN); siRNA OA1 #3: 5'- GGT TGT CGA ATA TCA TCA A -3' (Hs_GPR143_1_HP siRNA from QIAGEN); siRNA MART-1 #1: 5'- AAG ACG AAA TGG ATA CAG AGC -3' (25); siRNA MART-1 #2: 5'- TCC GCT AGC AGT ACT AAT CAT -3' (Hs_MLANA_7_HP from QIAGEN); . siRNA non-targeting control: 5'- AAT TCT CCG AAC GTG TCA CGT -3'.

Reagents and Antibodies

Primary antibodies: polyclonal anti-human OA1, raised against the C-terminus of the human OA1, similar to the previously published (4); polyclonal anti EGFP (Molecular Probes); monoclonal anti flag M2 antibody (SIGMA-Aldrich); polyclonal anti flag (SIGMA-Aldrich); monoclonal anti β-tubulin antibody (SIGMA-Aldrich); TA99 mouse anti-TYRP11 mAb (American Type Culture Collection; (47)) for immunofluoscence and immunogold labelling and monoclonal anti-Tyrp1 75kDa (Abcam) for western blotting; melanoma Ab-2 anti-Pmel17 (clone HMB50) (Lab Vision Corporation); mouse monoclonal anti-Pmel17 (clone HMB45) (Novocasta); Pep13h antibody was a kind gift from M.S.Marks (University of Pennsylvania, Philadelphia); monoclonal anti-MART-1 7c10 (ABCAM); rabbit anti mouse IgG was purchased from Dakopatt; polyclonal anti biotin (Polysciences Biovalley). Monoclonal anti-LAMP1 (BD Biosciences). Chloroquine, MG132 and Epoxomycin (SIGMA Aldrich);

DAMP (3-(2,4-dinitroanilino)-3′-amino-*N*-methyldipropylamine) (Invitrogen). Bovine Serum Albumin coupled to 5 nm gold particles (BSAG) and Protein A Gold conjugates were purchased from Cell Microscopy Center, Utrecht The Netherlands.

Cloning of OA1-tagged constructs

The human OA1 coding sequence was amplified by polymerase chain reaction (PCR) by using *Pfu* high fidelity DNA polymerase (Promega) and the following primers containing EcoRI and XhoI restriction sites: OA1fw:CG*GAATTC*ATGACCCAGGCAGGCCGG;OA1rw:CCG*CTCGAG*TCACACCTGGACAC GGAAG. The PCR product was digested by EcoRI and XhoI and subsequently cloned into EcoRI/XhoI-digested pcDNA3-flag vector to express OA1 with a Flag-tag at the C-terminus. The same PCR product was also cloned into pEGFP-N1 vector (Invitrogen) to express OA1 with an EGFP-tag at the C-terminus.

Quantitative Real time-PCR

Total RNA was extracted from siRNAs and control transfected MNT-1 cells using RNeasy MiniKit (Quiagen) according to the manufacturer's instructions. The same amount of cDNA was synthesized using Superscript II (Invitrogen) and random primers. Real time PCR was carried out with the GeneAmp 7000 Sequence Detection System (Applied Biosystem). The RT-PCR reaction was performed using cDNA, 12.5 μl SYBR green master mix (Applied Biosystem) and 400 nM primers for each gene (*see list below*). Water was added to a final reaction volume of 25 μl. The PCR conditions were as follows: preheating at 50°C for 2 min and 95°C for 10 min; 40 cycles of 15 s at 95°C and 1 min at 60°C.

Quantification results were expressed in terms of the cycle threshold (Ct). All real-time qPCR reactions were run in triplicate and the Ct values were averaged from three independent samples. Data were normalized to the internal control, the reference gene S26. Differences between the mean Ct values of each gene and those of the reference gene were calculated as $\Delta Ct = Ct_{gene} - Ct_{reference}$ and represented as $2^{-\Delta Ct}$.

Sequences of the forward (fw) and reverse (rw) intron-spanning primers used for Real-time qPCRs:

Human S26 fw	CCG TGC CTC CAA GAT GAC AA
Human S26 rw	GCA ATG ACG AAT TTC TTA ATG GCC T
Human OA1 fw	CGG AGA TCG GCA GGA CTG AGC AC

Human OA1 rw	ATA GTG GGG GAT GGC GTG GT
Human MART-1 fw	GAAGGGTTTGATCATCGGGA
Human MART-1 rw	GCATTGGGAACCACAGGTTC
Human Pmel17-fw	CAGCTCAGCCTTCACCATTA
Human Pmel17 rw	AAGTGCTTGTTCCCTCCATC

Immunoprecipitations and Western Blotting

siRNA treated MNT-1 cells at 80% of confluency and control MNT-1 cells were washed in cold PBS and lysed on ice in lysis buffer (50 mM Tris, 150 mM NaCl, 1% Triton X-100, 10 mM EDTA, pH 7,2 and protease inhibitor cocktail (Roche 11836153001). Lysates were then centrifuged at 21,000g for 20 min at 4°C. Protein concentrations were determined by Micro BCA™ Protein Assay Reagent Kit (Pierce). The protein samples were mixed with an equal volume of loading buffer containing 2% SDS (or 14% SDS for OA1) with 5% β-mercaptoethanol and then boiled for 2 min (or warmed 30 min at 37° for OA1 protein). For immunoprecipitation protein samples were first precleared using protein G agarose beads for 2 hrs at 4°C under rotation. Supernatants were collected and incubated with protein G agarose beads with 1 μg of rabbit anti-human IgG for 5 hrs at 4°C. To immunoprecipitate OA1, supernatants were incubated with 1 μg of anti-OA1 polyclonal antibody O/N at 4°C under rotation. As controls, 1 μg of rabbit anti-human IgG was used. After 10 washes in cold lysis buffer, immunoprecipitated proteins bound to the beads were incubated in sample buffer (containing 14% SDS for OA1 protein) and then boiled for 2 min (warmed 30 min at 37° for OA1 protein). Immunoprecipitated proteins were loaded and separated in 8% SDS-PAGE gel to reveal OA1 and in Nupage (4-12%) Bis-Tris gels (Invitrogen) to reveal the other proteins.

The separated proteins were then transfered to polyvinylidene difluoride membrane (Millipore) in XCell II™ Blot Module (Invitrogen) and the membranes were blocked in PBS/0.1%Tween-20 (PBS/T) with 5% non-fat dried milk, incubated with primary antibody in PBS/T, washed four times in blocking solution, and incubated with horseradish peroxidase-conjugated secondary antibody (anti-rabbit or anti-mouse; 1:10000; Jackson ImmunoResearch Laboratories) followed by washing in PBS/T. Visualization of the antibody binding was carried out with ECL Plus Western blotting detection system (GE Healthcare) according to the manufacturer's instruction. Signal intensities were quantified with Image J software.

Melanin assay

Cells were disrupted by sonication in 50 mM Tris-HCl, pH 7.4, 2 mM EDTA, 150 mM NaCl, 1 mM dithiothreitol and protease inhibitors. Pigment was pelleted at 20,000g for 15 min at 4°C, rinsed once in ethanol/ether (1:1), and dissolved in 2M NaOH/ 20% dimethylsulfoxide at 60°C. Melanin content was measured as optical density at 492 nm (48).

Immunofluorescence (IF)

Transfected MNT-1 cells on coverslips were rinsed in PBS and fixed for 15min in 4% paraformaldehyde/PBS at room temperature (RT). Fixed cells were washed in PBS and quenched 10 min in PBS/ 50 mM glycin, saturated in PBS/ 1 mg/ml BSA (blocking buffer) and permeabilized in PBS/ 0.05% saponin/ 1 mg/ml BSA (incubation buffer, IB). Cells were incubated 1 hr with the primary antibody diluted in IB, washed three times in IB and incubated with the corresponding secondary antibody Alexa 488- or Alexa 568-conjugated anti-rabbit or anti-mouse secondary antibodies (1:200; Molecular probes) for 45 min in IB and washed again. Finally, coverslips were mounted in DABCO medium and examined on a Leica Microsystemes (Nanterre, France) DM-RXA2 3D deconvolution microscope equipped with a piezo z-drive (Physik Instrument, Pantin, France) and a 100x1.4NA-PL-APO objective lens for optical sectioning. Images are maximum-intensity z projections of 3D image stacks acquired using Metamorph software (MDS Analytical Technologies, Sunnyvale, CA) through a Coolsnap HQ (Photometrics Coolsnap HQ) cooled CCD-camera except images shown in fig 5B-I where single stacks were deconvoluted.

Electron Microscopy (EM)

For conventional EM, cells grown on coverslips were fixed with 2.5% glutaraldehyde in 0.1M cacodylate buffer for 24 hrs. After several washes with 0.1M cacodylate buffer, the cells were postfixed with 2% OsO4, dehydrated in ethanol, and embedded in Epon while on the coverslips. Ultrathin sections were prepared and counterstained with uranyl acetate and lead citrate before the observation. For quantification, melanosomes were counted on 10 randomly acquired micrographs at X5,000 of siOA1 and control MNT1 cells. The area of cell analyzed was determined by iTEM software and expressed in square micrometers (160μm^2).

For immunogold labelling, cells were fixed with a mixture of 2%PFA and 0.2% glutaraldehyde in 0.1M phosphate buffer, pH 7.4 and processed for ultracryomicrotomy as previously described (49). Ultrathin cryosections were single- or double-immunogold labelled with antibodies and protein A coupled to 5 or 10 or 15-nm gold, as indicated in the legends to the figures. Sections of resin embedded

cells and immunogold labeled cryosections were observed under a Philips CM120 electron microscope (FEI company), equipped with a KeenView camera (Soft Imaging System; SIS, Germany). For quantification of OA1 labeling, 500 gold particles (endogenous OA1) or 800 (transfected OA1) were counted in randomly selected cells profiles of cells in each of two experiments. Tyrp1 and LAMP1 gold particles were randomly counted in a total of 80 unpigmented (stage I/II) or pigmented (stage III/IV) melanosomes, in two separate experiments. Data are presented as mean ± SD.

Uptake of BSAG and DAMP

Uptake of the endocytic tracer BSAG and the weak base DAMP (3-(2,4-dinitroanilino)-3′-amino-*N*-methyldipropylamine) were performed on living cells before fixation and processing as previously reported (9). *Uptake of BSAG:* cells were washed with serum-free DMEM, pulsed for 10 min at 37° with BSAG (OD_{520nm}=5), washed with ice-cold medium/2%FBS and the endocytic tracer was chased for 45min. After washing with ice-cold medium, cells were fixed. *Incubation with DAMP:* cells were washed with serum-free DMEM and incubated with DAMP (30μM) for 15 min at 37°. Cells were washed with ice-cold medium and then fixed.

Funding

This work was supported by Institut Curie,CNRS, Fondation pour la Recherche Medicale (GR) and fellowships from Federico II University of Naples, EMBO short term and Institut Curie (to F.G.).

Acknowledgements

We thank D. Tenza, I. Hurbain, M. Romao, C. Delevoye, G. van Niel, S. Simoes for technical help and insightful discussions during the course of this work. We are indebted to M.S.Marks for helpful suggestions and critical reading of the manuscript. We are grateful to L. Cabanie for OA1 antibody purification (Plateforme de production de protéines recombinantes, Institut Curie, UMR144) and to V.Fraisier and L. Sengmanivong (PITC-IBiSA Imaging Facility, Institut Curie) for assistance with deconvolution microscopy.

Conflict of Interest:

The authors declare no conflict of interest

References

1. Cortese, K., Giordano, F., Surace, E.M., Venturi, C., Ballabio, A., Tacchetti, C. and Marigo, V. (2005) The ocular albinism type 1 (OA1) gene controls melanosome maturation and size. *Invest Ophthalmol Vis Sci,* **46,** 4358-64.
2. Incerti, B., Cortese, K., Pizzigoni, A., Surace, E.M., Varani, S., Coppola, M., Jeffery, G., Seeliger, M., Jaissle, G., Bennett, D.C. *et al.* (2000) Oa1 knock-out: new insights on the pathogenesis of ocular albinism type 1. *Hum Mol Genet.,* **9,** 2781-2788.
3. Schiaffino, M.V., Baschirotto, C., Pellegrini, G., Montalti, S., Tacchetti, C., De Luca, M. and Ballabio, A. (1996) The ocular albinism type 1 gene product is a membrane glycoprotein localized to melanosomes. *Proc. Natl. Acad. Sci. USA,* **93,** 9055-9060.
4. Schiaffino, M.V., d'Addio, M., Alloni, A., Baschirotto, C., Valetti, C., Cortese, K., Puri, C., Bassi, M.T., Colla, C., De Luca, M. *et al.* (1999) Ocular albinism: evidence for a defect in an intracellular signal transduction system. *Nat Genet,* **23,** 108-12.
5. Innamorati, G., Piccirillo, R., Bagnato, P., Palmisano, I. and Schiaffino, M.V. (2006) The melanosomal/lysosomal protein OA1 has properties of a G protein-coupled receptor. *Pigment Cell Res,* **19,** 125-35.
6. Lopez, V.M., Decatur, C.L., Stamer, W.D., Lynch, R.M. and McKay, B.S. (2008) L-DOPA is an endogenous ligand for OA1. *PLoS Biol,* **6,** e236.
7. Samaraweera, P., Donatien, P.D., Qazi, S., Kobayashi, T., Hearing, V.J., Panthier, J.J. and Orlow, S.J. (1999) Identification and characterization of a melanocyte-specific novel 65-kDa peripheral membrane protein. *Eur. J. Biochem.,* **266,** 924-934.
8. Bassi, M.T., Bergen, A.A., Wapenaar, M.C., Schiaffino, M.V., van Schooneveld, M., Yates, J.R., Charles, S.J., Meitinger, T. and Ballabio, A. (1994) A submicroscopic deletion in a patient with isolated X-linked ocular albinism (OA1). *Hum Mol Genet,* **3,** 647-8.
9. Raposo, G., Tenza, D., Murphy, D.M., Berson, J.F. and Marks, M.S. (2001) Distinct protein sorting and localization to premelanosomes, melanosomes, and lysosomes in pigmented melanocytic cells. *J Cell Biol,* **152,** 809-24.
10. Raposo, G. and Marks, M.S. (2007) Melanosomes--dark organelles enlighten endosomal membrane transport. *Nat Rev Mol Cell Biol,* **8,** 786-97.
11. Seiji, M., Fitzpatrick, T.M., Simpson, R.T. and Birbeck, M.S.C. (1963) Chemical composition and terminology of specialized organelles (melanosomes and melanin granules) in mammalian melanocytes. *Nature,* **197,** 1082-1084.
12. Seiji, M., Fitzpatrick, T.B. and Birbeck, M.S. (1961) The melanosome: a distinctive subcellular particle of mammalian melanocytes and the site of melanogenesis. *J Invest Dermatol,* **36,** 243-52.
13. Lee, Z.H., Hou, L., Moellmann, G., Kuklinska, E., Antol, K., Fraser, M., Halaban, R. and Kwon, B.S. (1996) Characterization and subcellular localization of human Pmel 17/*silver*, a 100-kDa (pre)melanosomal membrane protein associated with 5,6,-dihydroxyindole-2-carboxylic acid (DHICA) converting activity. *J. Invest. Dermatol.,* **106,** 605-610.
14. Hurbain, I., Geerts, W.J., Boudier, T., Marco, S., Verkleij, A.J., Marks, M.S. and Raposo, G. (2008) Electron tomography of early melanosomes: Implications for melanogenesis and the generation of fibrillar amyloid sheets. *Proc Natl Acad Sci U S A,* **105,** 19726-19731.

15. Berson, J.F., Harper, D., Tenza, D., Raposo, G. and Marks, M.S. (2001) Pmel17 initiates premelanosome morphogenesis within multivesicular bodies. *Mol. Biol. Cell,* **12,** 3451-3464.
16. Berson, J.F., Theos, A.C., Harper, D.C., Tenza, D., Raposo, G. and Marks, M.S. (2003) Proprotein convertase cleavage liberates a fibrillogenic fragment of a resident glycoprotein to initiate melanosome biogenesis. *J Cell Biol,* **161,** 521-33.
17. Theos, A.C., Berson, J.F., Theos, S.C., Herman, K.E., Harper, D.C., Tenza, D., Sviderskaya, E.V., Lamoreux, M.L., Bennett, D.C., Raposo, G. *et al.* (2006) Dual loss of ER export and endocytic signals with altered melanosome morphology in the silver mutation of Pmel17. *Mol Biol Cell,* **17,** 3598-612.
18. Yamamoto, O. and Bhawan, J. (1994) Three modes of melanosome transfers in Caucasian facial skin: hypothesis based on an ultrastructural study. *Pigment Cell Res.,* **7,** 158-169.
19. Van Den Bossche, K., Naeyaert, J.M. and Lambert, J. (2006) The quest for the mechanism of melanin transfer. *Traffic,* **7,** 769-78.
20. Fowler, D.M., Koulov, A.V., Alory-Jost, C., Marks, M.S., Balch, W.E. and Kelly, J.W. (2006) Functional amyloid formation within mammalian tissue. *PLoS Biology,* **4,** 100-107.
21. Theos, A.C., Truschel, S.T., Tenza, D., Hurbain, I., Harper, D.C., Berson, J.F., Thomas, P.C., Raposo, G. and Marks, M.S. (2006) A lumenal domain-dependent pathway for sorting to intralumenal vesicles of multivesicular endosomes involved in organelle morphogenesis. *Dev Cell,* **10,** 343-54.
22. De Maziere, A.M., Muehlethaler, K., Van Donselaar, E., Salvi, S., Davoust, J., Cerottini, J.C., Levy, F., Slot, J.W. and Rimoldi, D. (2002) The Melanocytic Protein Melan-A/MART-1 Has a Subcellular Localization Distinct from Typical Melanosomal Proteins. *Traffic,* **3,** 678-93.
23. Levy, F., Muehlethaler, K., Salvi, S., Peitrequin, A.L., Lindholm, C.K., Cerottini, J.C. and Rimoldi, D. (2005) Ubiquitylation of a melanosomal protein by HECT-E3 ligases serves as sorting signal for lysosomal degradation. *Mol Biol Cell,* **16,** 1777-87.
24. Truschel, S.T., Simoes, S., Setty, S.R.G., Harper, D.C., Tenza, T., Thomas, P.C., Herman, K.E., Sackett, S.D., Cowan, D.C., Theos, A.C. *et al.* (2009) ESCRT-I function is required for Tyrp-1 transport from early endosomes to the melanosome limiting membrane. *Traffic,* **In press**.
25. Hoashi, T., Watabe, H., Muller, J., Yamaguchi, Y., Vieira, W.D. and Hearing, V.J. (2005) MART-1 is required for the function of the melanosomal matrix protein PMEL17/GP100 and the maturation of melanosomes. *J Biol Chem,* **280,** 14006-16.
26. Piccirillo, R., Palmisano, I., Innamorati, G., Bagnato, P., Altimare, D. and Schiaffino, M.V. (2006) An unconventional dileucine-based motif and a novel cytosolic motif are required for the lysosomal and melanosomal targeting of OA1. *J Cell Sci,* **119,** 2003-14.
27. Hoek, K., Rimm, D.L., Williams, K.R., Zhao, H., Ariyan, S., Lin, A., Kluger, H.M., Berger, A.J., Cheng, E., Trombetta, E.S. *et al.* (2004) Expression profiling reveals novel pathways in the transformation of melanocytes to melanomas. *Cancer Res,* **64,** 5270-82.
28. Yasumoto, K., Watabe, H., Valencia, J.C., Kushimoto, T., Kobayashi, T., Appella, E. and Hearing, V.J. (2004) Epitope mapping of the melanosomal matrix protein gp100 (PMEL17): rapid processing in the endoplasmic reticulum and glycosylation in the early Golgi compartment. *J Biol Chem,* **279,** 28330-8.

29. Valencia, J.C., Watabe, H., Chi, A., Rouzaud, F., Chen, K.G., Vieira, W.D., Takahashi, K., Yamaguchi, Y., Berens, W., Nagashima, K. *et al.* (2006) Sorting of Pmel17 to melanosomes through the plasma membrane by AP1 and AP2: evidence for the polarized nature of melanocytes. *J Cell Sci,* **119,** 1080-91.
30. Harper, D.C., Theos, A.C., Herman, K.E., Tenza, D., Raposo, G. and Marks, M.S. (2007) Premelanosome amyloid-like fibrils are composed of only golgi-processed forms of pmel17 that have been proteolytically processed in endosomes. *J Biol Chem*.
31. Kummer, M.P., Maruyama, H., Huelsmann, C., Baches, S., Weggen, S. and Koo, E.H. (2009) Formation of Pmel17 Amyloid Is Regulated by Juxtamembrane Metalloproteinase Cleavage, and the Resulting C-terminal Fragment Is a Substrate for {gamma}-Secretase. *J. Biol.Chem.,* **284,** 2296-2306.
32. Ohkuma, S. and Poole, B. (1978) Fluorescence probe measurement of the intralysosomal pH in living cells and the perturbation of pH by various agents. *Proc Natl Acad Sci U S A,* **75,** 3327-31.
33. Gonzalez-Noriega, A., Grubb, J.H., Talkad, V. and Sly, W.S. (1980) Chloroquine inhibits lysosomal enzyme pinocytosis and enhances lysosomal enzyme secretion by impairing receptor recycling. *J Cell Biol,* **85,** 839-52.
34. Rock, K.L., Gramm, C., Rothstein, L., Clark, K., Stein, R., Dick, L., Hwang, D. and Goldberg, A.L. (1994) Inhibitors of the proteasome block the degradation of most cell proteins and the generation of peptides presented on MHC class I molecules. *Cell,* **78,** 761-71.
35. Dick, L.R., Cruikshank, A.A., Grenier, L., Melandri, F.D., Nunes, S.L. and Stein, R.L. (1996) Mechanistic studies on the inactivation of the proteasome by lactacystin: a central role for clasto-lactacystin beta-lactone. *J Biol Chem,* **271,** 7273-6.
36. Sin, N., Kim, K.B., Elofsson, M., Meng, L., Auth, H., Kwok, B.H. and Crews, C.M. (1999) Total synthesis of the potent proteasome inhibitor epoxomicin: a useful tool for understanding proteasome biology. *Bioorg Med Chem Lett,* **9,** 2283-8.
37. Lee, D.H. and Goldberg, A.L. (1998) Proteasome inhibitors: valuable new tools for cell biologists. *Trends Cell Biol,* **8,** 397-403.
38. Tanowitz, M. and Von Zastrow, M. (2002) Ubiquitination-independent trafficking of G protein-coupled receptors to lysosomes. *J Biol Chem,* **277,** 50219-22.
39. Huizing, M., Helip-Wooley, A., Westbroek, W., Gunay-Aygun, M. and Gahl, W.A. (2008) Disorders of lysosome-related organelle biogenesis: clinical and molecular genetics. *Annu Rev Genomics Hum Genet,* **9,** 359-86.
40. Kushimoto, T., Basrur, V., Valencia, J., Matsunaga, J., Vieira, W.D., Ferrans, V.J., Muller, J., Appella, E. and Hearing, V.J. (2001) A model for melanosome biogenesis based on the purification and analysis of early melanosomes. *Proc. Natl. Acad. Sci. U.S.A.,* **98,** 10698-10703.
41. Oetting, W.S. and King, R.A. (1999) Molecular basis of albinism: mutations and polymorphisms of pigmentation genes associated with albinism. *Human Mutation,* **13,** 99-115.
42. Palmisano, I., Bagnato, P., Palmigiano, A., Innamorati, G., Rotondo, G., Altimare, D., Venturi, C., Sviderskaya, E.V., Piccirillo, R., Coppola, M. *et al.* (2008) The ocular albinism type 1 protein, an intracellular G protein-coupled receptor, regulates melanosome transport in pigment cells. *Hum Mol Genet,* **17,** 3487-501.

43. Margeta-Mitrovic, M., Jan, Y.N. and Jan, L.Y. (2000) A trafficking checkpoint controls GABA(B) receptor heterodimerization. *Neuron,* **27,** 97-106.
44. Terrillon, S. and Bouvier, M. (2004) Roles of G-protein-coupled receptor dimerization. *EMBO Rep,* **5,** 30-4.
45. Shenoy, S.K. (2007) Seven-transmembrane receptors and ubiquitination. *Circ Res,* **100,** 1142-54.
46. Martin, N.P., Lefkowitz, R.J. and Shenoy, S.K. (2003) Regulation of V2 vasopressin receptor degradation by agonist-promoted ubiquitination. *J Biol Chem,* **278,** 45954-9.
47. Thomson, T.M., Mattes, M.J., Roux, L., Old, L.J. and Lloyd, K.O. (1985) Pigmentation-associated glycoprotein of human melanomas and melanocytes: definition with a mouse monoclonal antibody. *J. Invest. Dermatol.,* **85,** 169-174.
48. Wasmeier, C., Romao, M., Plowright, L., Bennett, D.C., Raposo, G. and Seabra, M.C. (2006) Rab38 and Rab32 control post-Golgi trafficking of melanogenic enzymes. *J Cell Biol,* **175,** 271-81.
49. Slot, J.W. and Geuze, H.J. (2007) Cryosectioning and immunolabeling. *Nat Protoc,* **2,** 2480-91.

Legends to Figures

Figure 1.

Localization of OA1 in MNT-1 cells. Ultrathin cryosections of MNT-1 cells were double immunogold labeled with anti-OA1 and anti-Tyrp1 (A and B) or anti-OA1 and anti-Pmel17 (C and D) or anti-OA1 and anti-LAMP1 (E). (A) OA1 (PAG 15) is detected in the limiting membrane (arrows) and in small intraluminal vesicles (arrowhead) of pigmented Tyrp1 (PAG10)- positive melanosomes. (B) Note the presence of OA1 in the membrane of vesicles close to melanosomes (arrowhead). (C and D) Pmel17 (PAG 5)-positive compartments (unpigmented fibrillar melanosomes) show high labeling for OA1 (PAG 10) (arrows fig 1C,D). (E) OA1 (PAG10) localizes to the limiting membrane of LAMP1 (PAG15) positive lysosomes (arrow) and to the membrane of internal vesicles of late endosomes (arrowheads). I, stage I. II, stage II. III, stage III. IV, stage IV. I/II, stage I/II. LE, late endosome. Lys, lysosome. Bars, 200 nm. (F) Quantification of gold particles labeling OA1 on ultrathin cryosections of MNT-1 cells. Results are presented as the percentage of the total number of gold particles for OA1 (PAG 10) in the distinct morphologically defined compartments. The highest labeling for OA1 is observed in stage II premelanosomes (24%).

Figure 2.

Inactivation of OA1 affects melanosome number, melanosome size and composition. MNT-1 cells were transfected with control (Ctrl) non-targeting siRNA or 3 different siRNAs targeting OA1 (siRNA#1,#2,#3) (A) Cell harvested five days after siRNA transfection were analyzed by real time qPCR. Real time qPCR reactions were performed in triplicate and averaged. Y-axis: $2^{(-dCT)}$ value represents differences between the mean Ct (cycle threshold) values of tested genes (OA1) and those of reference gene (S26). $2^{(-dCT)}$ values are significantly lower in MNT-1 cells interfered with oligo siOA1#3 and siOA1#2 (reduction of OA1 mRNA levels: 15% siRNA #1, 78% siRNA #2, 95% siRNA #3) than in the control. (B) Cells treated with OA1 or control siRNAs were analyzed by immunoblotting with the polyclonal anti-OA1 antibody and anti β-tubulin. OA1 appears as a doublet of 45-48kDa and a band at 60kDa corresponding to different patterns of glycosylation. The extra band at 65KD (asterisk) is a non-specific. OA1 protein levels are significantly reduced in cells interfered with siOA1#3 and siOA1#2. (C,D) OA1 distribution was analyzed by

immunofluorescence, using the polyclonal anti-OA1 antibody in control and in siOA1 treated cells (siOA1#2 or siOA1#3). OA1 expression is clearly reduced in most siOA1 treated cells. (E,F) Bright field images show the reduction of pigmentation in siOA1 treated cells, as compared to control cells. (G) Evaluation of melanin content in OA1 depleted cells shows a 50% decrease and as shown in Inset the decrease in pigmentation is visible in cell pellets (same number of OA1 depleted and control cells diluted in the same volume). Y-axis: Percentage (%) of Melanin content normalized to the control (assumed as 1%). (H,I) Cells treated with OA1 or control siRNAs were analyzed by conventional EM. Note the different stages of melanosomes in control cells (I,II,III,IV) (H) OA1 depleted cells display only few pigmented, normal sized melanosomes (IV) and show several "enlarged" organelles with different morphological features: melanosomal structures with disorganized fibrils (arrowhead), with melanin deposits (arrows) and aberrant mixed compartments (asterisk) containing fibrillar striations and melanin pigment (I). (L) Histogram representing the number of melanosomes (stage II+III+IV) per area (160μm^2) in control and siOA1 treated cells. Bars, 200 nm. (K) Number of different stage melanosomes in control and siOA1 cells. In siOA1 cells melanosomes were distinguished between normal (organized fibers, normal size), aberrant melanosomes (fibrils disorganized, bigger size) and mixed melanosomes. Melanosomes were counted on 10 randomly acquired micrographs at X5,000 of siOA1 and control MNT1 cells. The area of cell analyzed was determined by iTEM software and expressed in square micrometers (160μm^2).

Figure 3.

Localization of Tyrp1 and LAMP1 in OA1 depleted cells. Ultrathin cryosections of MNT-1 cells treated with control (Ctrl; A,C,E) or OA1 siRNA (siOA1; B,D,F,G,H) were double immunogold labeled for Tyrp1 (PAG10) and Pmel17 (PAG5)(A,B) or Tyrp1 (PAG10) and LAMP1 (PAG15)(C,D,E,F,G,H). Labeling for Tyrp1 is observed at the limiting membrane of mature pigmented melanosomes (A, arrows) but not in Pmel17 positive premelanosomes (arrowhead). Note a lysosome highly labeled for LAMP1 (C, arrow). (B) OA1 depleted cells show aberrant premelanosomes with disorganized fibrils and those are labeled for both Tyrp1 (arrows) and Pmel17 (arrowhead). (D-G) Note the labeling for LAMP1 on the membrane of melanosomes and pigmented enlarged compartments in siOA1 treated cells as compared to control (arrows). (H) LAMP1 was present also in Tyrp1 positive vacuolar structures

generated in OA1 depleted cells (arrows inset). II, stage II. IV, stage IV. Bars 200nm. (I) Western blot analysis of lysates of cells treated with control (Ctrl) and OA1 (siOA1) siRNAs using anti-Tyrp1 or anti-LAMP1 antibodies and anti-β-tubulin as a loading control. In siOA1 treated cells the expression of Tyrp1 is slightly increased whereas LAMP1 levels remain unchanged.

Table 1.

Quantitative analysis of Tyrp1 and LAMP1 distribution in different melanosomal stages in siOA1 and control cells.

Tyrp1 and LAMP1 gold particles were randomly counted in a total of 80 unpigmented (stage I/II) or pigmented (stage III/IV) melanosomes, in two separate experiments. Data are presented as mean ± SD. N, number of gold particles. % percentage of gold particles. In siOA1 cells melanosomes were distinguished between normal (organized fibers, normal size) and aberrant melanosomes (fibrils disorganized, bigger size).

Figure 4.

MART-1 depletion affects Pmel17 processing and melanosome biogenesis. (A) Western blot analysis of TX-soluble fraction extracted from cells treated with control (Ctrl) and OA1 (siO) siRNAs using anti-HMB45 (Aa) or pep13h (Ac) antibody directed against the processed forms and the C-terminal of Pmel17 respectively and anti-β-tubulin as a loading control. Note the accumulation of Malpha (Mα) fragment and the reduction of MalphaC (MαC) fragment in siOA1 lysates (Aa, arrows). TX-insoluble pellets (enriched in Mα, the luminal domain fragment of Pmel17) from siOA1 and control cells were re-extracted in TX lysis buffer containing 8M Urea at 60° and analysed by western blot using anti-HMB45 (Pmel17; Mα and MαC) antibody (Ab). The accumulation of Malpha (Mα) fragment and the reduction of MalphaC (MαC) are maintained. (B) Western blot analysis of lysates from cells treated with control (Ctrl) and MART-1 (siM) siRNAs using anti-MART-1 (Ba), anti-HMB45 (Bb) or pep13h (Bc) antibody against the processed forms and the C-terminal of Pmel17 respectively and anti-β-tubulin as a loading control. Note the accumulation of Malpha (Mα) fragment and the reduction of MalphaC (MαC) fragment in siMART-1 lysates (Bb, arrows). (C,D,E,F) Ultrathin cryosections of control and siMART-1 treated MNT-1 cells were single immunogold labeled for Pmel17 (HMB50; PAG 5) (C and D) or double immunogold labeled for Tyrp1 (PAG 10) and Pmel17 (HMB50; PAG 5) (E

and F). MART-1 depleted cells display aberrant enlarged compartments with a mixed content of Pmel17 positive fibrils and electron dense pigment (arrow in D). As shown in (F) in MART-1 depleted cells, Tyrp1 localizes to Pmel17 positive unpigmented melanosomal compartments. II, stage II. IV, stage IV. Bars 200 nm.

Figure 5.

OA1 and MART-1 co immunoprecipitate and co localize in Golgi and TGN

(A) MNT-1 cell lysates were immunoprecipitated with polyclonal anti-OA1 (IP OA1) or anti rabbit IgG (IP IgG rabbit) antibody. Immunoprecipitates were fractionated by SDS-PAGE and immunoblotted with anti-MART-1, Tyrp1 or OA1 antibody as indicated on the right of each panel. The arrow indicates a specific band detected by anti-MART-1 antibody in OA1-immunoprecipitates.

(B,C,D) MNT-1 cells were analyzed by immunofluorescence and deconvolution after double labeling for OA1 (B; green) and MART-1 (C; red). Overlap of the two images is shown in D and the phase (blue pseudocolored melanosomes) is shown in E. Magnified insets are also shown (F,G,H,I). Arrows indicate colocalization between OA1 and MART-1. (J,K,L) Ultrathin cryosections of MNT-1 cells were double immunogold labeled for OA1 and MART-1 and analyzed by EM. OA1 and MART-1 are detected in the Golgi and in associated vesicles (J, arrows), at the cytosolic side of small endosomes (K, arrow) and in multivesicular compartments (L, arrow). TGN, Trans Golgi Network. IV, stage IV. Bars 200 nm.

Figure 6

Depletion of MART-1 affects OA1 stability. MNT-1 cells were treated with control (Ctrl) siRNA or siRNA targeting MART-1 (siMART-1). (A-H) Immunofluorescence analysis of control (A,B,C,D) and siMART-1 cells (E,F,G,H) stained with anti-MART-1 (red) and anti-OA1 (green) antibodies. MART-1 depleted cells (arrow) show a clear decrease in OA1 labeling. Phase is shown in D and H. (I) Real Time quantitative PCR of MART-1 and OA1, in siMART-1 (siMART-1) and control (Ctrl) MNT1 cells. Note that MART-1 RNA is significantly decreased (94%) and OA1 RNA does not significantly change in siMART1 cells. Y-axis: $2^{(-dCT)}$ value represents differences between the mean Ct (cycle threshold) values of tested genes and those of reference gene (S26). (J) Western blot analysis of lysates of cells treated with control (Ctrl) and MART-1 (siM) siRNAs using anti-MART-1 or anti-OA1 antibody and anti-β-tubulin as a loading control. Note the depletion of MART-1 (90%) and the

reduction of OA1 protein (85%) in cells treated with MART-1 siRNA. Arrows point to the specific forms of OA1 (60 kDa and doublet 45-48 kDa). (K) Western blot analysis of control (Ctrl) and siMART-1 (siM) cells, treated with Chloroquine 200μM (Chlor, lysosome inhibitor)(Ka) or MG132 50 μM (MG132, proteasome inhibitor)(Kb) or Epoxomycin 10 μM (Epox, specific proteasome inhibitor)(Kc) for 5hrs, 5 days after siRNAs transfection. Control cells treated with Chloroquine show an increase in OA1 as compared to untreated control cells. OA1 levels increase also in siMART-1 cells treated with Chloroquine, as compared to untreated siMART-1. Note also the increase of OA1 in siMART-1 cells treated with MG132 and Epoxomycin as compared to the untreated inactivated cells. Arrows point to the specific forms of OA1 (60 kDa and doublet 45-48 kDa). Graphs shows signal intensity of OA1 normalized to β-tubulin in the different conditions of two separate experiments. Data are expressed as arbitrary units and presented as mean ± SD.

Supplementary Figures

Figure S1.

Localization of OA1-Flag in transfected MNT-1 cells. Ultrathin cryosections of MNT-1 cells transfected with OA1-Flag construct were double immunogold labeled with anti-Flag (OA1) and anti-Tyrp1 (A and B) or with anti-Flag (OA1) and anti-Pmel17 (C). (A and B) OA1-Flag (PAG 15) is present at the limiting membrane of Tyrp1-positive (PAG 10) pigmented melanosomes (arrows, A), in small intraluminal vesicles that are also labeled for Tyrp1 (arrowhead, A, B) and in intracellular small vesicles closed to melanosomes (asterisk, B). Note the presence of large electron lucent OA1-Flag positive membrane vacuoles (350 nm) labeled for Tyrp1 that localize at the proximity of melanosomes (asterisks, A). (C). OA1-Flag (PAG15) localizes to stage IV pigmented mature melanosomes (arrows) while stage II unpigmented premelanosomes do not show consistent labeling. Bars, 200 nm. (D) Quantitative analysis of the distribution of OA1-Flag in MNT-1 transfected cells. Results are presented as the percentage of the total number of counted gold particles for OA1 (PAG 15) in the distinct morphologically defined compartments in MNT-1 cells. The highest labeling for OA1 is observed in stage IV premelanosomes (23%).

Figure S2.

Aberrant melanosomes are generated in OA1 depleted MNT1 and in OA1 knock out mouse melanocytes. OA1 siRNA targeted or not targeted human MNT1 (siOA1; A,B,C) and OA1 Knock-out (melan-OA1-/-) or wild type (melan-a) mouse melanocytes (D,E) were analyzed by conventional EM (A,B,D,E) or after double immunogold labeling for Tyrp1 (PAG 15) and Pmel17 (PAG 5) on ultrathin cryosections (C). (A) Electron micrograph showing a siOA1 targeted cell (defined on the base of the typical phenotype) close to a siOA1 not targeted cell. Melanosomes in the siOA1 targeted cell display disorganized luminal fibrils and are 3 times bigger than in the not targeted cell (arrows). I, stage I. II, stage II. III, stage III. IV, stage IV. Bar: 1 µm. (B) OA1 depleted cells show aberrant melanosome displaying electron dense pigment surrounded by fibrils characteristic of immature premelanosomes. These fibrils are labeled for Pmel17 (arrows, C). Bars 200 nm. (D,E) Electron micrographs of regions of the cytoplasm of OA1 Knockout (melan-Oa1$^{-/-}$; E) and wild type (melan-a; D) melanocytes. Arrows indicate aberrant pigmented compartments with a mixed content in OA1 Knockout cells. Insets are 2,5X magnification of areas showing representative melanosomes. II, stage II. III, stage III. IV, stage IV. Bars 200nm.

Figure S3

(A,B) Control (Ctrl) or OA1 siRNA (siOA1) treated MNT1 cells were pulsed with BSAG (5nm) for 10 min and the endocytic tracer was chased at 37°C for 45 min. BSAG is present in MVBs (arrowheads, A-B) located close to melanosomes labeled for Tyrp1 (arrows, A-B). The enlarged melanosomal organelles in siOA1 cells were not accessed by the BSAG (B). (C,D) Control (Ctrl) and OA1 depleted (siOA1) MNT1 cells were incubated with DAMP for 15 min at 37°C and then fixed, processed and double immunogold labeled for Tyrp1 (PAG10) and DAMP, visualized with anti-DNP antibody (PAG 5). The weak base DAMP accumulates primarily in stage II melanosomes while stage IV melanosomes show less labeling. The enlarged melanosomal organelles (arrow, D) in siOA1 cells appear to be correctly acidified. III, stage III. II/III, stage II/III. IV, stage IV. Bars 200 nm.

Figure S4

(A) Real Time quantitative PCR of OA1, Pmel17 and MART-1 and in siOA1 treated (siOA1) and control (Ctrl) MNT1 cells. Y-axis: $2^{(-dCT)}$ value represents differences between the mean Ct (cycle threshold) values of tested genes and those of reference gene (S26). Pmel17 and MART-1 RNA levels do not change in siOA1 cells. (B) Western blot analysis of lysates of cells treated with control (Ctrl) and OA1 (siOA1) siRNAs using anti-MART-1 and anti-β-tubulin as a loading control. MART-1 does not significatively change in siOA1 treated cells vs control.

Table 1

	Tyrp1			
	stage I/ II	stage I/ II	stage III/IV	stage III/IV
	n	%	n	%
Ctrl	36 ±5	8%	448 ±19	92%
siOA1 (normal melanosomes)	206 ±11	27%	554 ±22	73%
siOA1 (aberrant melanosomes)	471 ±17	36%	833 ±30	64%

	LAMP1			
	stage I/ II	stage I/ II	stage III/IV	stage III/IV
	n	%	n	%
Ctrl	16 ±4	25%	48 ± 7	75%
siOA1 (normal melanosomes)	33 ±8	29%	79 ±12	71%
siOA1 (aberrant melanosomes)	100 ±14	35%	186 ±20	65%

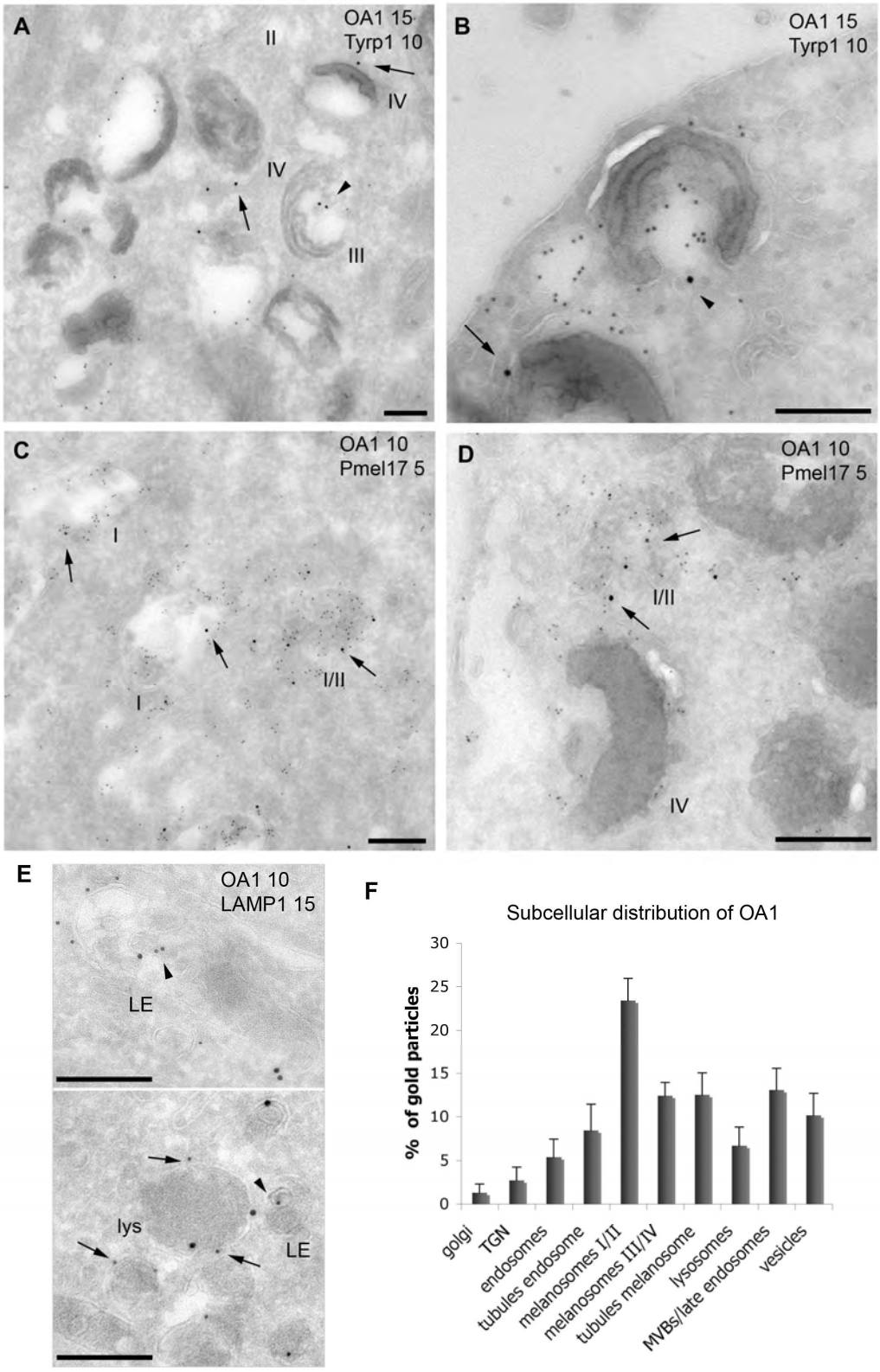
A
OA1 15
Tyrp1 10
II
IV
IV
III
B
OA1 15
Tyrp1 10
C
OA1 10
Pmel17 5
I
I/II
I
D
OA1 10
Pmel17 5
I/II
IV
E
OA1 10
LAMP1 15
LE
lys
LE
F
Subcellular distribution of OA1
% of gold particles
0
5
10
15
20
25
30
golgi
TGN
endosomes
tubules endosome
melanosomes I/II
melanosomes III/IV
tubules melanosome
lysosomes
MVBs/late endosomes
vesicles

Figure 1

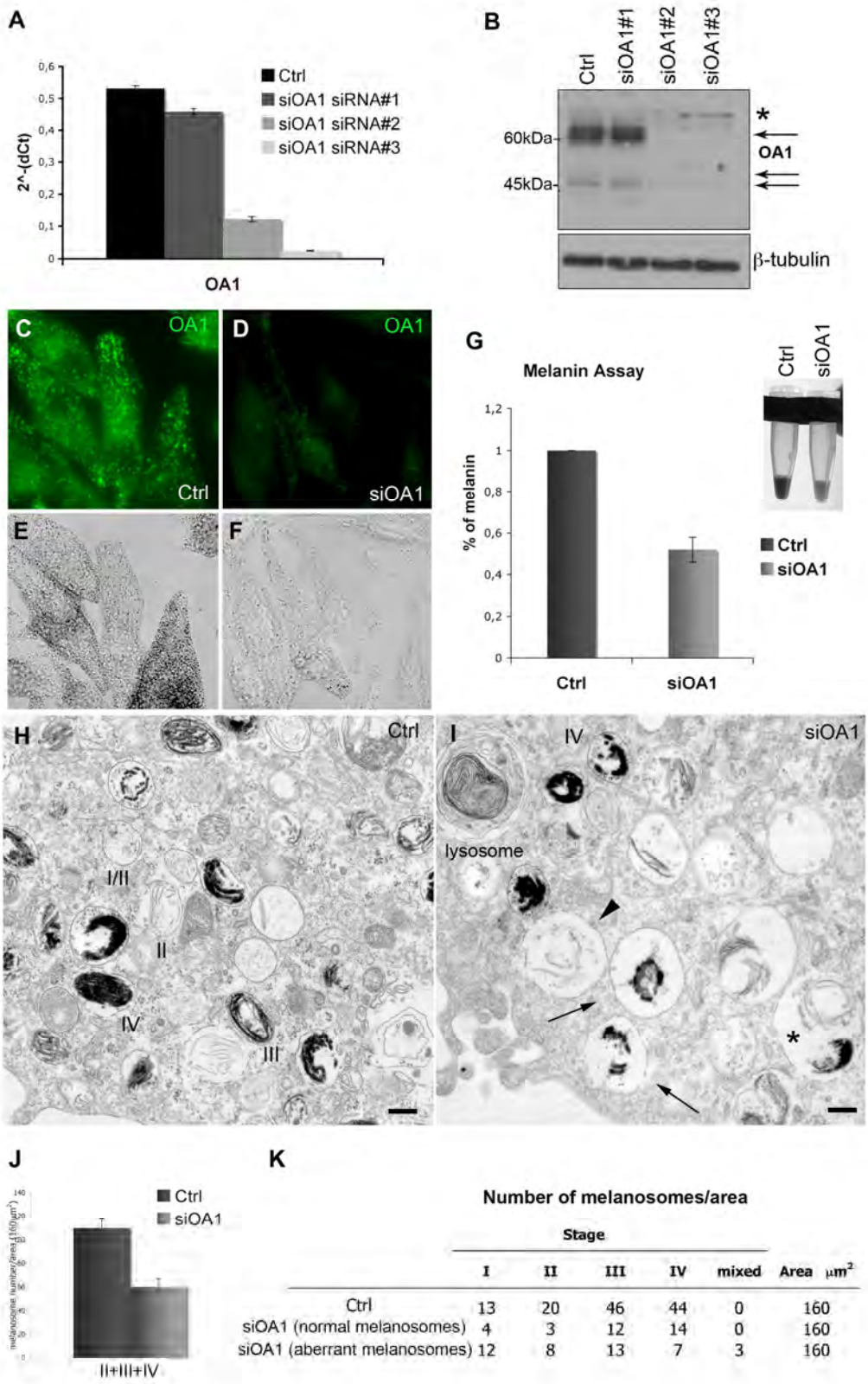

	Stage					
	I	II	III	IV	mixed	Area μm^2
Ctrl	13	20	46	44	0	160
siOA1 (normal melanosomes)	4	3	12	14	0	160
siOA1 (aberrant melanosomes)	12	8	13	7	3	160

Figure 2

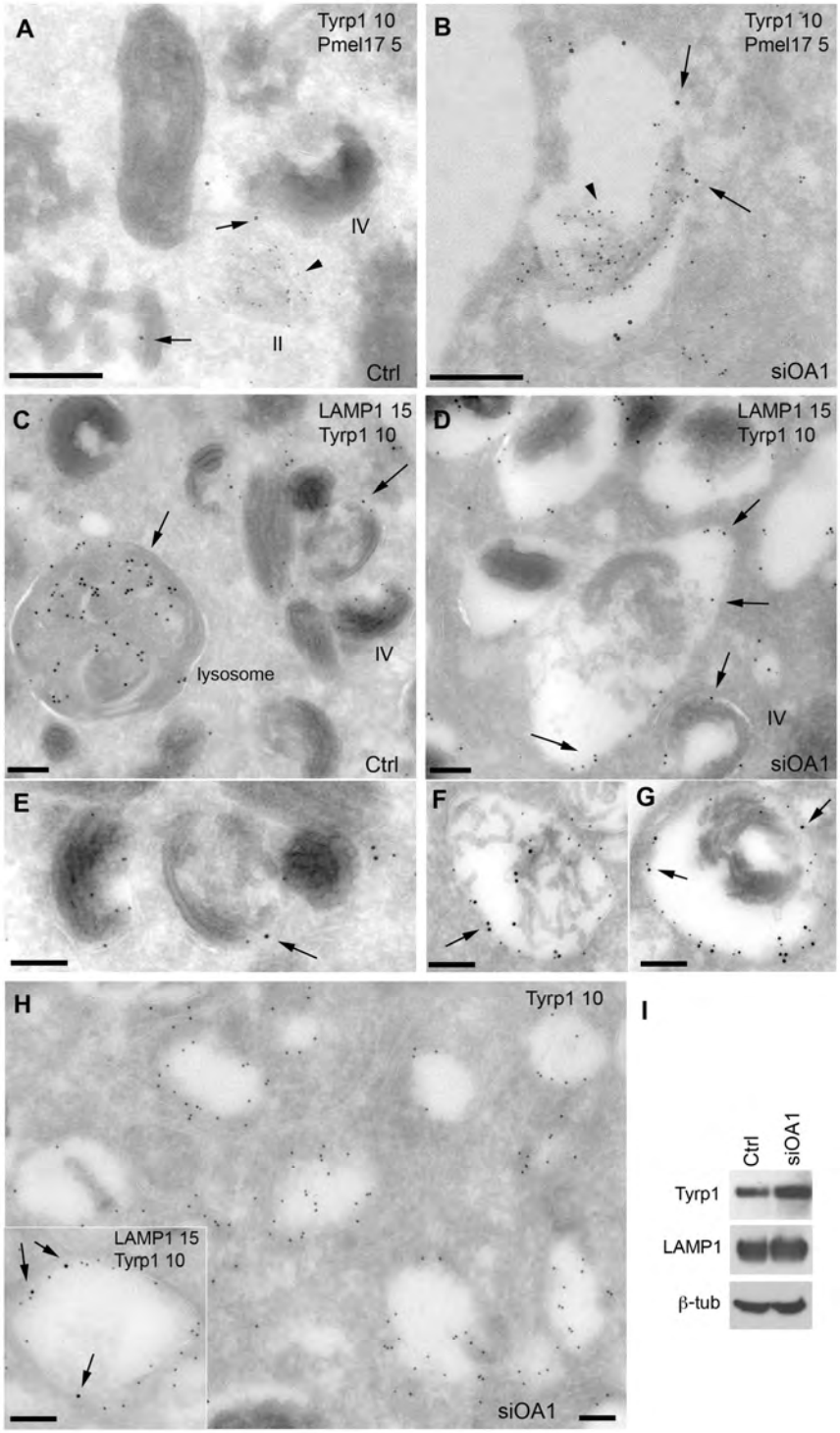
A
Tyrp1 10
Pmel17 5
IV
II
Ctrl
B
Tyrp1 10
Pmel17 5
siOA1
C
LAMP1 15
Tyrp1 10
lysosome
IV
Ctrl
D
LAMP1 15
Tyrp1 10
IV
siOA1
E
F
G
H
Tyrp1 10
LAMP1 15
Tyrp1 10
siOA1
I
Ctrl
siOA1
Tyrp1
LAMP1
β-tub

Figure 3

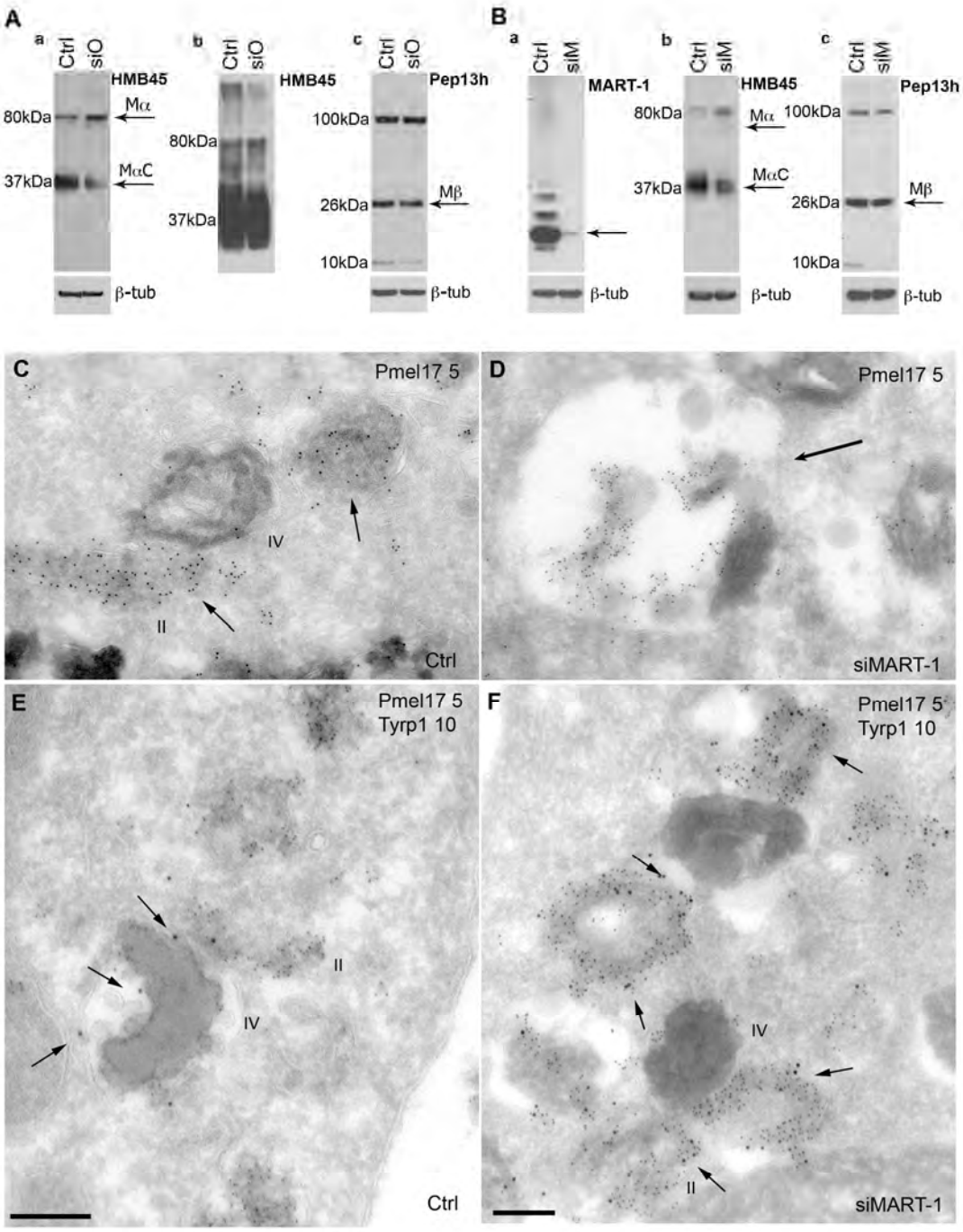
A
a
Ctrl
siO
HMB45
Mα
80kDa
37kDa
MαC
β-tub
b
Ctrl
siO
HMB45
80kDa
37kDa
c
Ctrl
siO
Pep13h
100kDa
26kDa
10kDa
Mβ
β-tub
B
a
Ctrl
siM
MART-1
β-tub
b
Ctrl
siM
HMB45
80kDa
Mα
37kDa
MαC
β-tub
c
Ctrl
siM
Pep13h
100kDa
26kDa
10kDa
Mβ
β-tub
C
Pmel17 5
IV
II
Ctrl
D
Pmel17 5
siMART-1
E
Pmel17 5
Tyrp1 10
II
IV
Ctrl
F
Pmel17 5
Tyrp1 10
IV
II
siMART-1

Figure 4

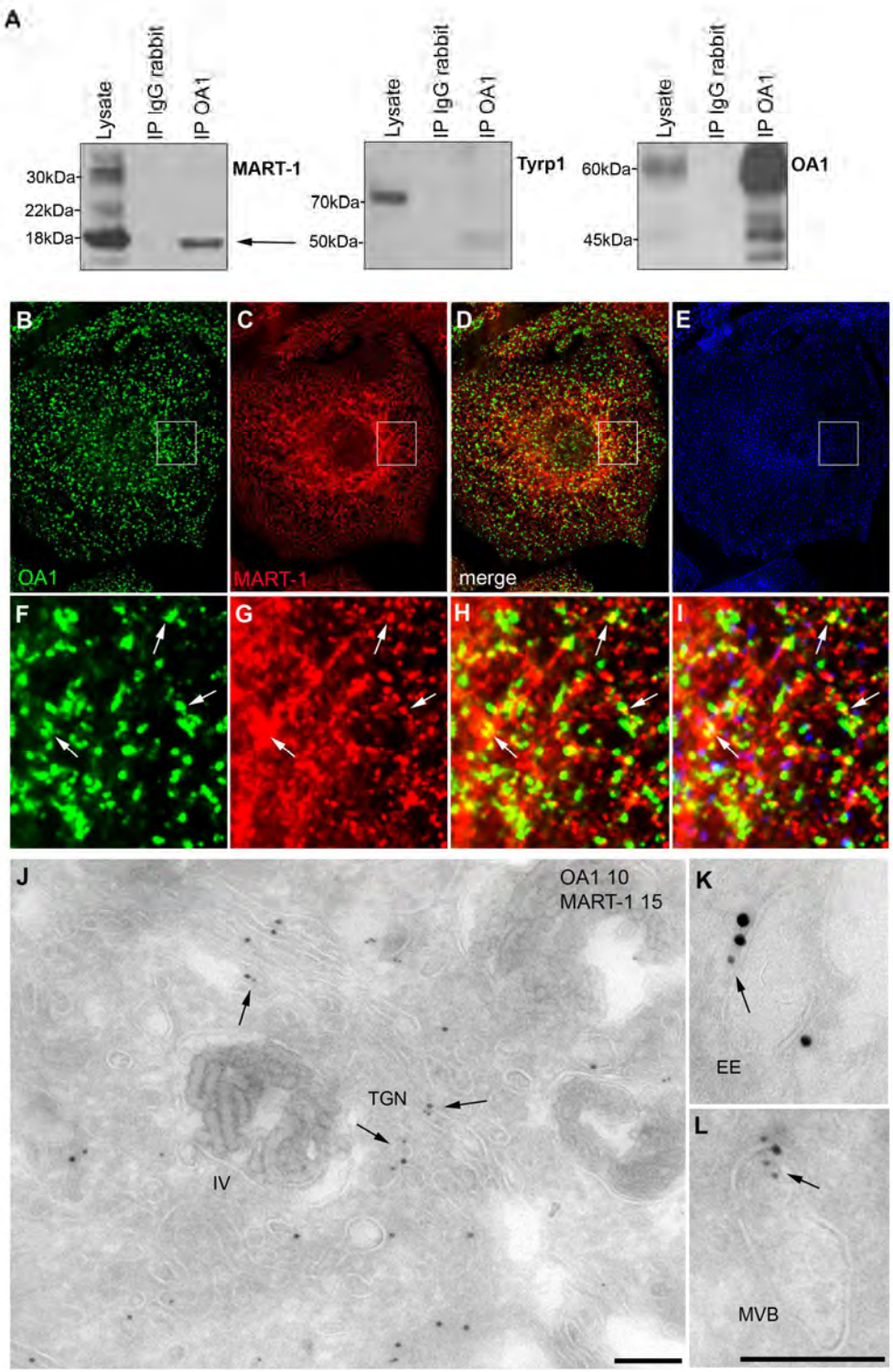
A
Lysate
IP IgG rabbit
IP OA1
30kDa
22kDa
18kDa
MART-1
Lysate
IP IgG rabbit
IP OA1
70kDa
50kDa
Tyrp1
Lysate
IP IgG rabbit
IP OA1
60kDa
45kDa
OA1
B
OA1
C
MART-1
D
merge
E
F
G
H
I
J
OA1 10
MART-1 15
TGN
IV
K
EE
L
MVB

Figure 5

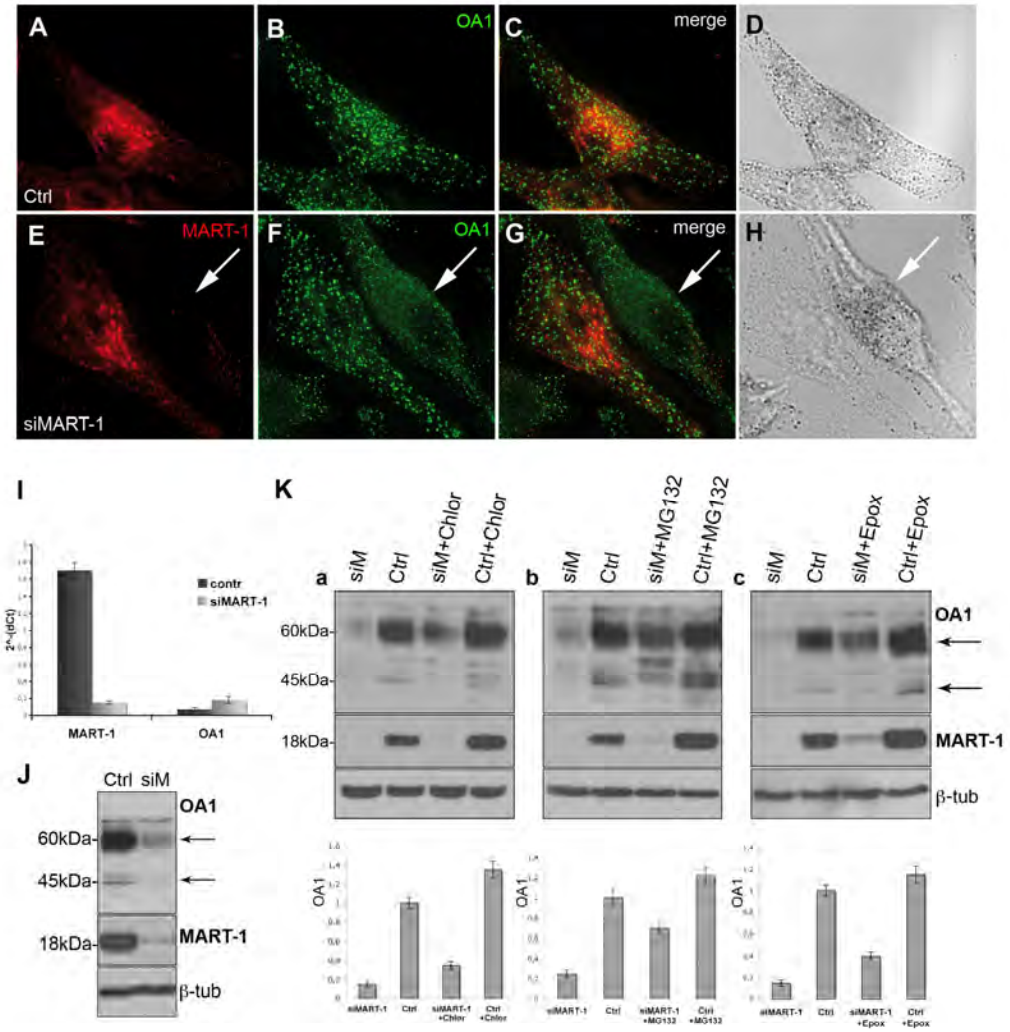
A
B
OA1
C
merge
D
Ctrl
E
MART-1
F
OA1
G
merge
H
siMART-1
I
contr
siMART-1
MART-1
OA1
J
Ctrl siM
OA1
60kDa-
45kDa-
18kDa-
MART-1
β-tub
K
a
siM
Ctrl
siM+Chlor
Ctrl+Chlor
b
siM
Ctrl
siM+MG132
Ctrl+MG132
c
siM
Ctrl
siM+Epox
Ctrl+Epox
60kDa-
45kDa-
18kDa-
OA1
MART-1
β-tub

Figure 6

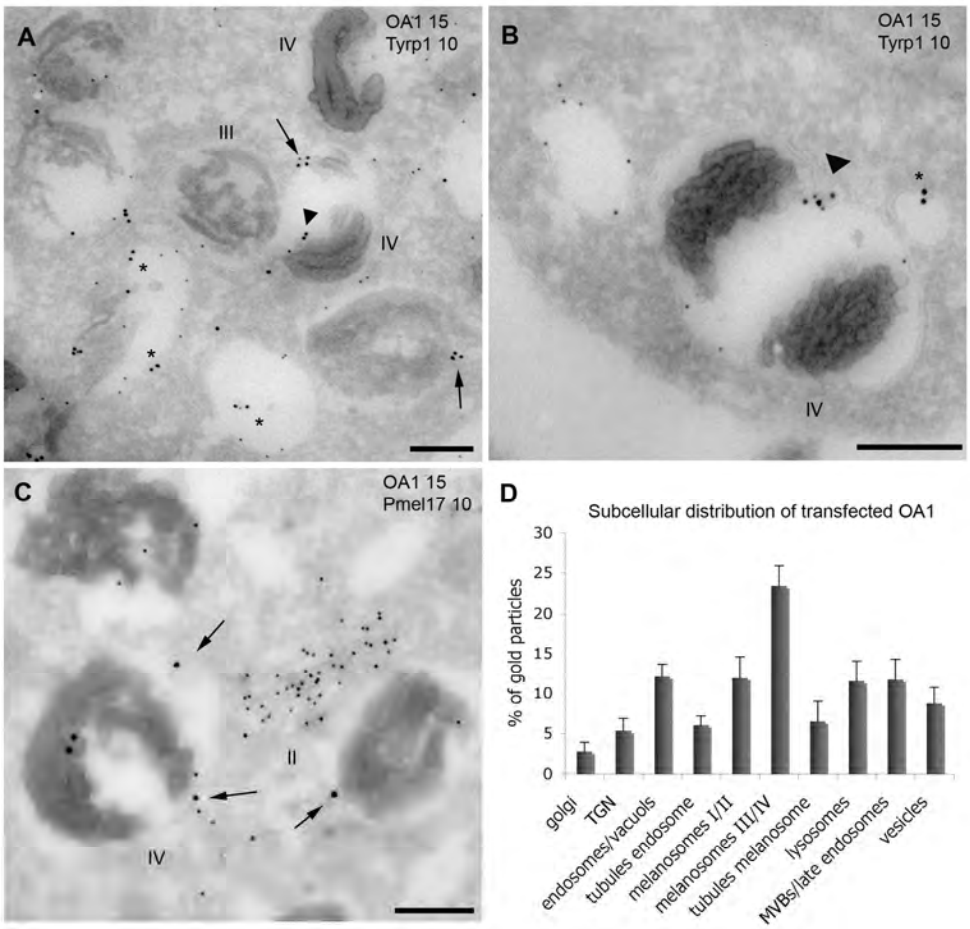

Supplementary Figure 1

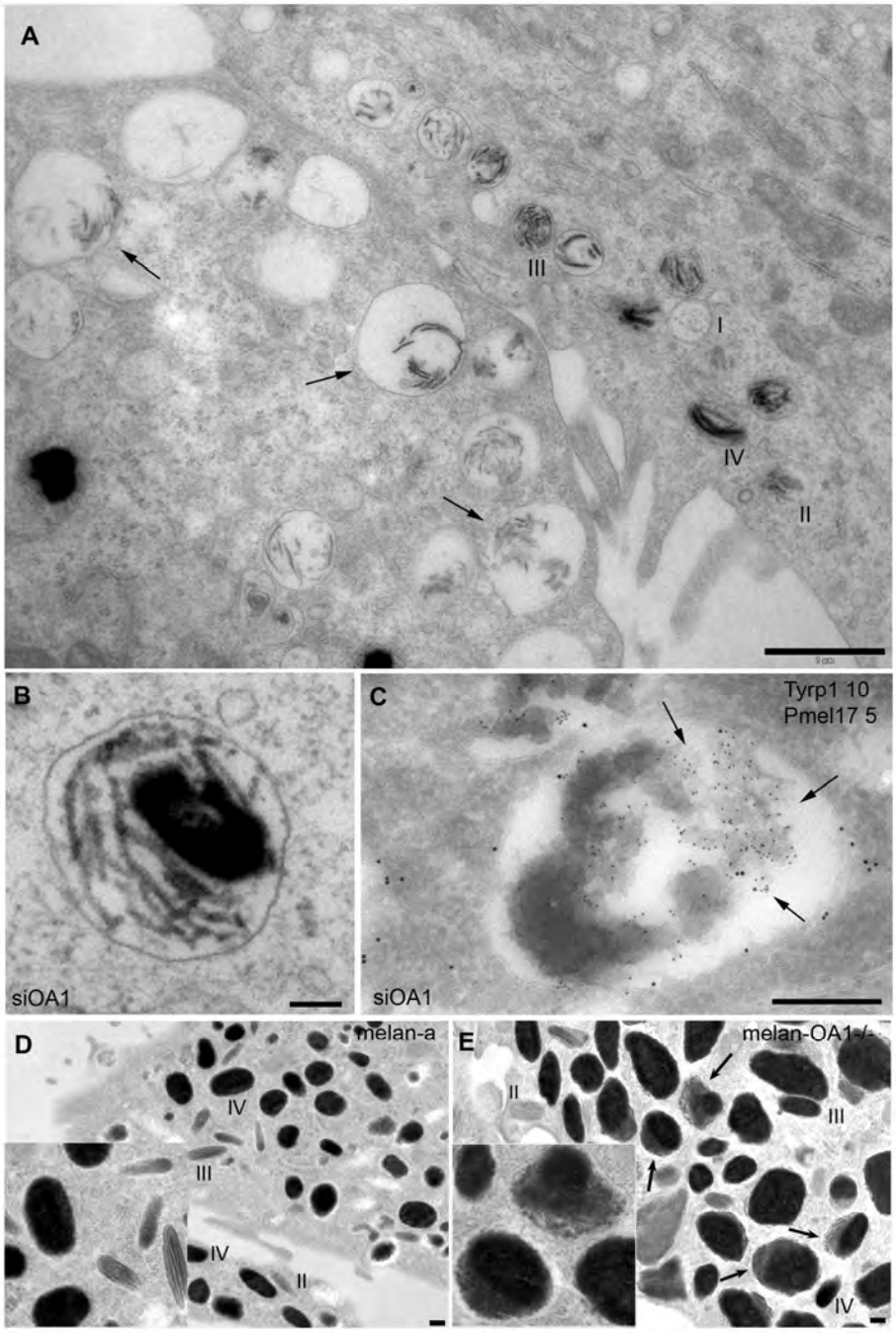

Supplemntary Figure 2

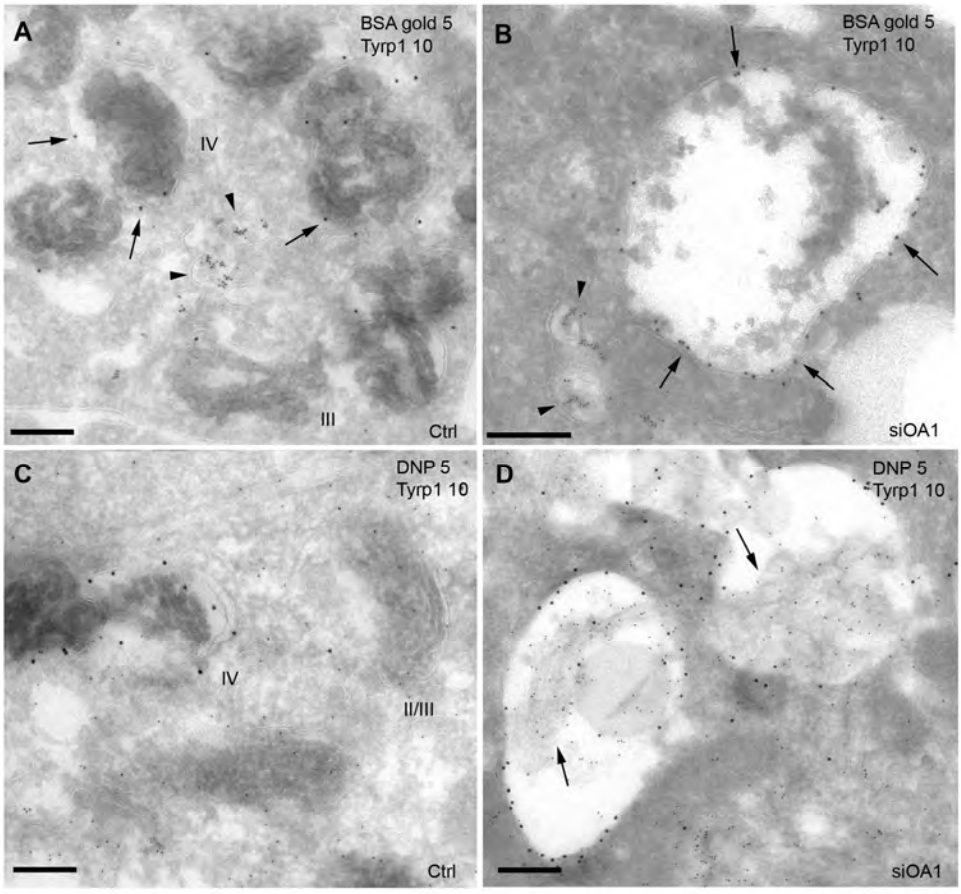

Supplementary Figure 3

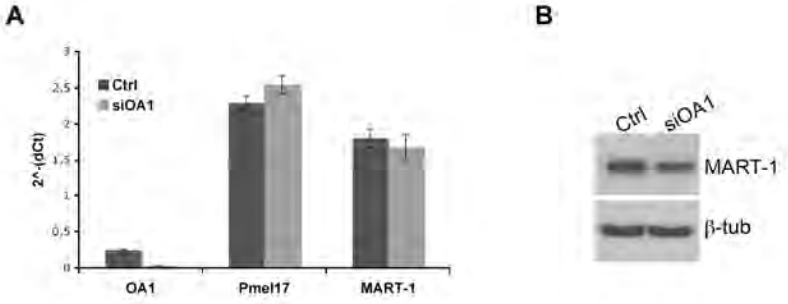

Supplementary Figure 4